Geochemistry Geophysics Geosystems G3

*Article*
Volume 13, Number 3
20 March 2012
Q03014, doi:10.1029/2011GC003812
ISSN: 1525-2027

Published by AGU and the Geochemical Society

# Compositional diversity of Mauna Kea shield lavas recovered by the Hawaii Scientific Drilling Project: Inferences on source lithology, magma supply, and the role of multiple volcanoes

**J. Michael Rhodes**
*Department of Geosciences, University of Massachusetts, Amherst, Massachusetts 01003, USA (jmrhodes@geo.umass.edu)*

**Shichun Huang**
*Department of Earth and Planetary Sciences, Harvard University, Cambridge, Massachusetts 02138, USA*

**Frederick A. Frey and Malcolm Pringle**
*Earth Atmospheric and Planetary Sciences Department, Massachusetts Institute of Technology, Cambridge, Massachusetts 02139, USA*

**Guangping Xu**
*Department of Geosciences, Colorado State University, Fort Collins, Colorado 80523, USA*

[1] The final Stage (Phase-2) of the Hawaii Scientific Drilling Project (HSDP) recovered 408 m of basaltic core (3098–3506 mbsl) attributed to Mauna Kea volcano. We determined the major and trace element composition of 40 samples from this core. Our results show that the incompatible element ratios, such as Zr/Nb, which are correlated with Pb isotopic ratios, are more variable in the lower 408 m of Mauna Kea shield lavas than in the overlying 2855 m (~450 ka). We argue that this geochemical diversity was present in the mantle source of Mauna Kea shield lavas and does not require the inter-fingering of lavas from adjacent volcanoes. Because of uncertainties in Ni partitioning between olivine and melt and the wide range of Ni contents in peridotites, we show that all Mauna Kea lavas may have been derived from a peridotite source. We also obtained major and trace element compositions for 24 whole-rock clasts and hyaloclastites and 7 glasses from HSDP Phase-1 core between 1767 and 1808 mbs. These enigmatic lavas, previously recognized by the distinctive high CaO and $K_2O$ contents of their glasses, are also relatively enriched in highly incompatible trace elements. We show that this group of lavas have affinities with post-shield lavas and argue that they are a consequence of lower degrees of melting (~a factor of two) than other Mauna Kea shield lavas, thereby providing evidence that magma supply varied significantly during the growth of the Mauna Kea shield.

**Components:** 17,100 words, 14 figures, 8 tables.

**Keywords:** Hawaiian volcanism; Mauna Kea; mantle plume.

**Index Terms:** 1033 Geochemistry: Intra-plate processes (3615, 8415); 1037 Geochemistry: Magma genesis and partial melting (3619); 1065 Geochemistry: Major and trace element geochemistry.

**Received** 28 July 2011; **Revised** 19 January 2012; **Accepted** 27 January 2012; **Published** 20 March 2012.

Rhodes, J. M., S. Huang, F. A. Frey, M. Pringle, and G. Xu (2012), Compositional diversity of Mauna Kea shield lavas recovered by the Hawaii Scientific Drilling Project: Inferences on source lithology, magma supply, and the role of multiple volcanoes, *Geochem. Geophys. Geosyst.*, *13*, Q03014, doi:10.1029/2011GC003812.

## 1. Introduction

[2] A major impediment to understanding the magmatic history of Hawaiian volcanoes and the structure of the Hawaiian mantle plume is the lack of thick stratigraphic sections that sample most of the 800 to 1500 ka of volcano growth [e.g., *Moore and Clague*, 1992; *Lipman*, 1995; *Garcia et al.*, 1995]. Subaerial sections of Hawaiian volcanoes reveal only a small fraction (5–10%) of this history and are biased toward the late stages of volcano growth. The Hawaii Scientific Drilling Project (HSDP) made a significant advance toward addressing this problem by drilling and coring a 1 km pilot hole, HSDP-1 [*Stolper et al.*, 1996], followed by a 3.1 km hole (HSDP-2) [*Garcia et al.*, 2007; *Stolper et al.*, 2009], on the eastern flank of Mauna Kea volcano. This international, multidisciplinary study documented ~450 ka (~209–647 ka) of Mauna Kea's magmatic history [*Sharp and Renne*, 2005], which began with a vigorous submarine shield-building stage, and ended with a marked decline in magma production as the volcano reached its post-shield stage [see *Stolper et al.*, 2009, Figure 6].

[3] Major results of the HSDP include information on the internal structure of a large oceanic volcano [*Garcia et al.*, 2007], varying magma compositions erupted during the shield building stage [e.g., *Huang and Frey*, 2003; *Rhodes and Vollinger*, 2004; *Stolper et al.*, 2004], and the isotopic diversity of the lavas [e.g., *Blichert-Toft et al.*, 2003; *Eisele et al.*, 2003; *Kurz et al.*, 2004; *Bryce and DePaolo*, 2005; *Blichert-Toft and Albarède*, 2009]. The geochemical heterogeneity of the lavas requires either heterogeneity in their source, or perhaps the HSDP core contains lavas erupted from several volcanoes [e.g., *Holcomb et al.*, 2000; *Blichert-Toft and Albarède*, 2009]. These HSDP results have significantly contributed to recent discussions of the nature and structure of mantle plumes [e.g., *Abouchami et al.*, 2005; *Bryce and DePaolo*, 2005; *Farnetani and Hofmann*, 2009, 2010; *Huang et al.*, 2011; *Weis et al.*, 2011] and the relative roles of peridotite and pyroxenite as sources of plume-related magmas [e.g., *Sobolev et al.*, 2005; *Herzberg*, 2006, 2011; *Putirka et al.*, 2011].

[4] Phase-1 of HSDP-2 (we use the terminology of *Stolper et al.* [2009, see Figure 3]) recovered 3100 m of core, documenting about 450 ka of Mauna Kea's eruptive history between 209 and 647 ka [*Sharp and Renne*, 2005; *Stolper et al.*, 2009]. Here, we report on the composition and geochemical stratigraphy of an additional 408 m of core (3098–3506 mbsl) recovered during Phase-2 (2003–2007) of the HSDP-2 project [*Stolper et al.*, 2009]. Assuming an eruption rate of 9 m/ka [see *Stolper et al.*, 2009, Figure 6], this 408 m of core extends the eruptive history of Mauna Kea by an additional 48 ka from 647 to 695 ka. The forty analyzed Phase-2 samples are from 33 of the 45 identified flow and intrusive units and consist mostly of submarine pillow lavas, with lesser amounts of hyaloclastites, pillow breccias, and massive volcanic and intrusive units (Figure 1a).

[5] We also sampled and determined whole-rock major and trace element abundances for 24 clasts and hyaloclastites from HSDP-2 Phase-1 flow units 248, 254, 255 and 256 higher in the core between 1767 and 1808 m (Figure 1b). These lavas, recognized previously by the distinctive major element compositions of glasses, were designated $CaO$-$K_2O$-rich glasses because of their high $CaO$ and $K_2O$ content relative to other Mauna Kea glasses [*Stolper et al.*, 2004]. Additionally, we determined trace element abundances in 7 of these high $CaO$-$K_2O$ glasses previously analyzed for major elements by *Stolper et al.* [2004]. In a provocative paper, *Herzberg* [2006] suggested that these $CaO$-$K_2O$ rich shield lavas may be the only Mauna Kea shield magmas derived from a peridotitic source and that all other shield lavas result from melting of pyroxenite sources.

[6] In this paper we use published and newly obtained geochemical data to show that the compositional diversity of lavas from the deepest part of the core (3098–3506 mbsl) exceeds that of younger lavas at higher stratigraphic levels. We also assess: (1) the roles of peridotite and pyroxenite in the source of Mauna Kea magmas; (2) the possibility that the HSDP core includes Mauna Kea shield lavas intermingled with lavas derived from other shields;

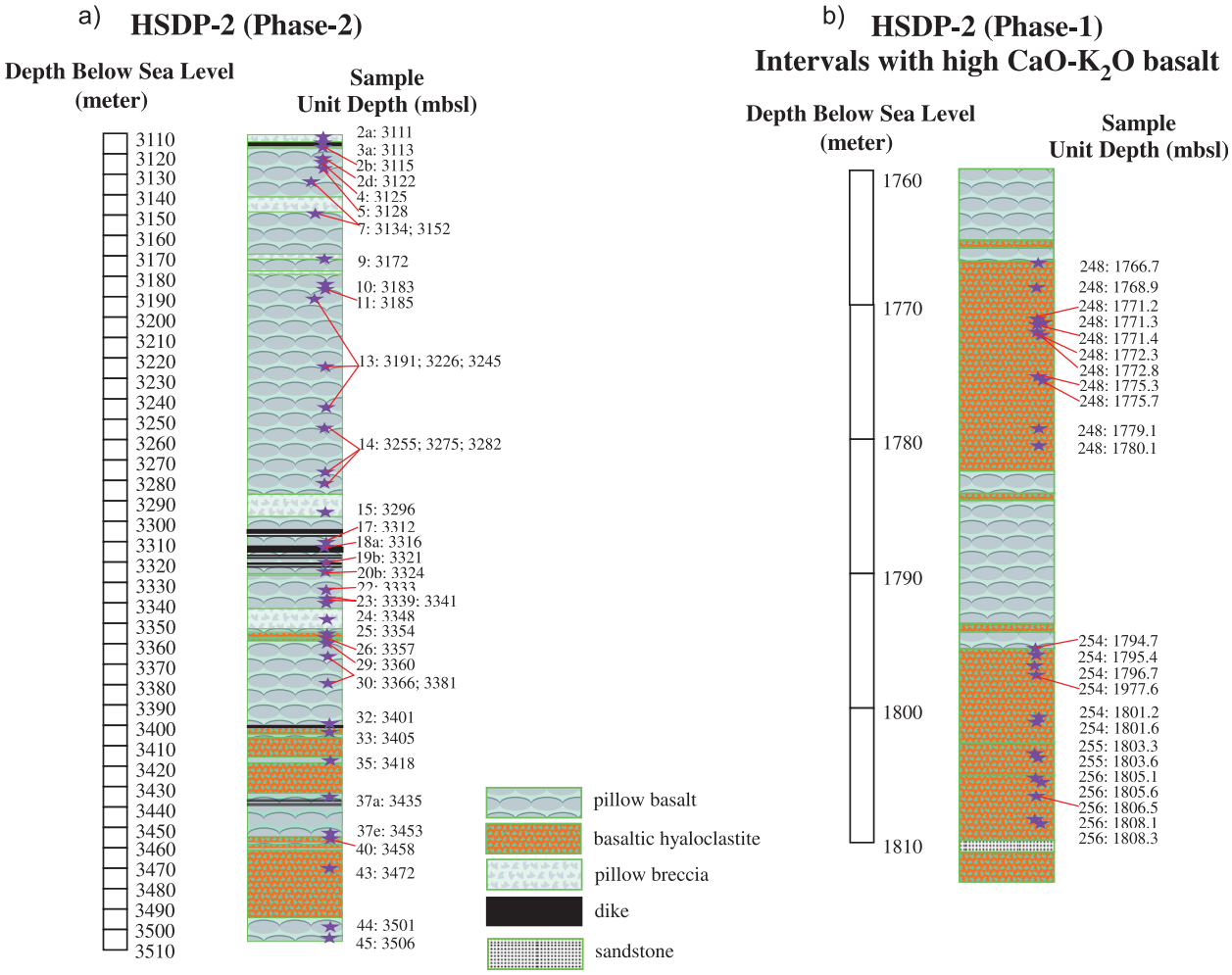


**Figure 1.** Simplified lithological sections of the Hawaii Scientific Drilling Project (HSDP) core, showing rock types, sample locations, flow unit numbers and depth in mbsl. (a) Core from Phase-2 of the project between 3098 and 3506 mbsl. (b) Core from Phase-1 of the project between 1767 and 1808 mbsl showing the location of High CaO-$K_2O$ whole-rock samples.

and (3) the origin of the enigmatic CaO-$K_2O$-rich lavas erupted in the depth interval of 1767 to 1808 m.

## 2. Analytical Methods

### 2.1. X-Ray Fluorescence Analysis of Whole-Rocks

[7] Tables 1a and 1b report the whole-rock major and trace element compositions of 40 Phase-2 lavas. Twenty eight of these are pillow lavas, or pillow breccia, 10 are massive units, including both volcanic and intrusive, and 2 are hyaloclastites. The sampling density for the Phase-2 lavas is around 9 m/sample, roughly twice the 19 m/sample of Phase-1 lavas by *Rhodes and Vollinger* [2004], and three times (~26 m/sample) that of the Phase-1 reference samples distributed to different laboratories. Tables 2a and 2b contain whole-rock major and trace element compositions of 24 High CaO lavas from Phase-1 of the core, between 1767 and 1808 mbsl. The sampling density is about 1.7 m/sample. Nine of these samples are hyaloclastites and 15 are clasts from within this hyaloclastite sequence.

[8] The sample crushing and washing protocols were identical to those described by *Rhodes* [1996], and the X-ray fluorescence (XRF) analytical methods for major and trace elements are described by *Rhodes and Vollinger* [2004]. Estimates of the precision and accuracy of these data are given by *Rhodes* [1996] and *Rhodes and Vollinger* [2004]. In addition to the customary major and trace elements

**Table 1a.** XRF Major Element Analyses of Lavas Sampled by Phase-2 of the HSDP Core[a]

| Run and Core Interval | Unit | Depth (mbsl) | Rock Type | $SiO_2$ (%) | $TiO_2$ (%) | $Al_2O_3$ (%) | $Fe_2O_3$* (%) | MnO (%) | MgO (%) | CaO (%) | $Na_2O$ (%) | $K_2O$ (%) | $P_2O_5$ (%) | Total (%) | Mg# | LOI (%) | Alkalic Index |
|---|---|---|---|---|---|---|---|---|---|---|---|---|---|---|---|---|---|
| R6-0.85-1.2 | 2a | 3098 | PI | 50.31 | 2.58 | 13.15 | 12.37 | 0.17 | 7.75 | 10.62 | 2.39 | 0.48 | 0.25 | 100.07 | 0.58 | 0.75 | −1.30 |
| R6-2.15-3.0 | 3 | 3098.2 | MI | 47.31 | 2.32 | 11.98 | 13.02 | 0.17 | 12.67 | 9.59 | 1.91 | 0.95 | 0.20 | 100.12 | 0.68 | 5.65 | −0.19 |
| R8-0.15-0.7 | 2b | 3102.4 | PI | 50.35 | 2.50 | 13.17 | 12.34 | 0.17 | 7.96 | 10.67 | 2.33 | 0.31 | 0.24 | 100.04 | 0.59 | 0.91 | −1.54 |
| R10-4.35-5.7 | 2d | 3109.4 | PI | 50.37 | 2.60 | 13.15 | 12.45 | 0.18 | 7.71 | 10.76 | 2.37 | 0.39 | 0.25 | 100.23 | 0.58 | 0.72 | −1.43 |
| R11-5.3-5.7 | 4 | 3111.5 | PB | 50.37 | 2.59 | 13.15 | 12.46 | 0.18 | 7.72 | 10.76 | 2.35 | 0.37 | 0.25 | 100.20 | 0.58 | 0.86 | −1.46 |
| R13-0.1-0.5 | 5 | 3115.2 | PI | 50.24 | 2.55 | 13.13 | 12.42 | 0.17 | 7.77 | 10.63 | 2.49 | 0.33 | 0.25 | 99.99 | 0.58 | −4.46 | −1.32 |
| R16-5.2-6.0 | 7 | 3122.5 | PI | 50.27 | 2.54 | 13.12 | 12.52 | 0.17 | 8.01 | 10.60 | 2.35 | 0.31 | 0.25 | 100.14 | 0.58 | 0.92 | −1.49 |
| R30-4.25-5.2 | 7 | 3141.2 | PI | 50.26 | 2.52 | 12.92 | 12.48 | 0.18 | 8.16 | 10.58 | 2.40 | 0.30 | 0.24 | 100.04 | 0.59 | 1.10 | −1.44 |
| R51-2.4-3.6 | 9 | 3160.8 | PI | 50.39 | 2.53 | 12.90 | 12.60 | 0.18 | 8.03 | 10.60 | 2.46 | 0.36 | 0.25 | 100.30 | 0.58 | 0.80 | −1.37 |
| R56-1.0-1.5 | 10 | 3171.1 | PB | 50.24 | 2.56 | 13.04 | 12.54 | 0.18 | 7.86 | 10.71 | 2.27 | 0.34 | 0.25 | 99.99 | 0.58 | 0.86 | −1.53 |
| R57-5.0-5.9 | 11 | 3173.4 | PI | 50.20 | 2.54 | 13.13 | 12.53 | 0.17 | 7.91 | 10.65 | 2.28 | 0.33 | 0.25 | 99.99 | 0.58 | 1.04 | −1.51 |
| R60-7.6-8.4 | 13 | 3181.2 | PI | 50.42 | 2.55 | 12.77 | 12.70 | 0.18 | 8.14 | 10.65 | 2.28 | 0.37 | 0.24 | 100.30 | 0.59 | 0.65 | −1.55 |
| R80-2.8-3.5 | 13 | 3215.5 | PI | 50.32 | 2.48 | 13.04 | 12.51 | 0.17 | 8.00 | 10.74 | 2.35 | 0.32 | 0.23 | 100.16 | 0.58 | 0.70 | −1.50 |
| R93-1.4-2.0 | 13 | 3234.7 | PI | 50.06 | 2.48 | 12.96 | 12.48 | 0.17 | 7.97 | 10.70 | 2.35 | 0.33 | 0.24 | 99.73 | 0.58 | 0.75 | −1.40 |
| R101-4.4-4.9 | 14 | 3244.8 | MV | 50.27 | 2.42 | 13.07 | 12.34 | 0.16 | 8.10 | 10.63 | 2.28 | 0.40 | 0.23 | 99.90 | 0.59 | 0.60 | −1.47 |
| R108-0.0-0.7 | 14 | 3263.9 | MV | 50.65 | 2.63 | 13.07 | 12.64 | 0.18 | 7.42 | 10.54 | 2.41 | 0.46 | 0.26 | 100.25 | 0.56 | 0.34 | −1.42 |
| R112-7.1-7.7 | 14 | 3277.0 | MV | 50.23 | 2.41 | 12.90 | 12.50 | 0.18 | 7.91 | 10.81 | 2.35 | 0.41 | 0.23 | 99.93 | 0.58 | 0.45 | −1.37 |
| R116-6.25-7.2 | 15 | 3285.8 | PI | 50.40 | 2.42 | 13.06 | 12.37 | 0.18 | 8.11 | 10.87 | 2.40 | 0.28 | 0.23 | 100.31 | 0.59 | 0.79 | −1.52 |
| R122-1.85-2.65 | 17 | 3300.1 | PI | 50.76 | 2.74 | 13.67 | 12.38 | 0.17 | 6.60 | 10.68 | 2.65 | 0.34 | 0.27 | 100.24 | 0.54 | 0.61 | −1.34 |
| R125-4.9-5.3 | 18a | 3305.9 | MI | 50.39 | 2.54 | 12.99 | 12.56 | 0.18 | 7.90 | 10.63 | 2.49 | 0.33 | 0.24 | 100.25 | 0.58 | 0.90 | −1.37 |
| R127-1.4-2.2 | 19b | 3308.2 | PI | 50.41 | 2.59 | 13.74 | 12.25 | 0.17 | 6.94 | 10.99 | 2.42 | 0.31 | 0.24 | 100.07 | 0.55 | 1.14 | −1.47 |
| R129-5.8-6.5 | 20b | 3313.5 | MI | 49.75 | 2.13 | 11.93 | 11.81 | 0.17 | 11.74 | 9.91 | 2.19 | 0.30 | 0.20 | 100.13 | 0.69 | 0.36 | −1.46 |
| R149-1.2-1.6 | 22 | 3333.3 | PI | 50.73 | 2.59 | 13.82 | 12.27 | 0.18 | 6.75 | 10.88 | 2.13 | 0.36 | 0.25 | 99.95 | 0.55 | 0.46 | −1.83 |
| R154-2.1-2.95 | 23 | 3339.5 | MV | 48.25 | 1.73 | 10.46 | 12.78 | 0.19 | 15.64 | 8.83 | 1.78 | 0.27 | 0.16 | 100.08 | 0.73 | 1.10 | −1.35 |
| R155-2.7-3.5 | 23 | 3341.4 | MV | 47.88 | 1.87 | 9.87 | 12.56 | 0.18 | 17.42 | 8.44 | 1.37 | 0.10 | 0.18 | 99.88 | 0.75 | 2.26 | −1.79 |
| R158-1.75-2.10 | 24 | 3348.3 | PB | 50.78 | 2.60 | 13.82 | 12.31 | 0.19 | 6.83 | 11.04 | 1.64 | 0.30 | 0.25 | 99.75 | 0.55 | 0.79 | −2.40 |
| R162-1.55-2.3 | 25 | 3353.9 | PI | 50.67 | 2.58 | 13.81 | 12.18 | 0.18 | 6.85 | 10.85 | 2.10 | 0.37 | 0.24 | 99.83 | 0.55 | 0.76 | −1.83 |
| R163-2.1-2.6 | 26 | 3357.0 | HY | 49.63 | 2.41 | 12.33 | 12.61 | 0.19 | 9.66 | 11.05 | 1.44 | 0.31 | 0.23 | 99.85 | 0.63 | 0.57 | −2.17 |
| R165-0.75-1.45 | 29 | 3359.8 | PI | 49.24 | 2.35 | 12.38 | 12.50 | 0.18 | 9.72 | 10.99 | 1.87 | 0.28 | 0.22 | 99.74 | 0.63 | 1.18 | −1.61 |
| R168-3.7-4.15 | 30 | 3366.3 | PI | 49.62 | 2.39 | 12.32 | 12.67 | 0.19 | 9.61 | 10.89 | 1.91 | 0.31 | 0.22 | 100.13 | 0.63 | 0.55 | −1.68 |
| R176-5.93-6.5 | 30 | 3381.3 | PI | 49.45 | 2.39 | 12.29 | 12.64 | 0.19 | 9.55 | 10.77 | 1.93 | 0.34 | 0.22 | 99.77 | 0.62 | 0.35 | −1.57 |
| R184-1.15-2.1 | 32 | 3400.9 | MI | 47.56 | 2.33 | 12.08 | 13.14 | 0.19 | 12.30 | 10.10 | 2.06 | 0.14 | 0.21 | 100.11 | 0.67 | 1.82 | −0.94 |
| R187-0.9-2.5 | 33 | 3405.3 | PI | 48.58 | 1.89 | 10.50 | 12.05 | 0.18 | 15.74 | 8.85 | 1.80 | 0.16 | 0.18 | 99.92 | 0.74 | 0.63 | −1.56 |
| R192-4.4-5.4 | 35 | 3418.1 | MV | 47.09 | 1.77 | 8.99 | 12.31 | 0.18 | 20.26 | 7.60 | 1.36 | 0.20 | 0.17 | 99.93 | 0.78 | 0.32 | −1.41 |
| R198-0.5-1.9 | 37a | 3435.2 | PI | 47.07 | 1.59 | 8.81 | 12.42 | 0.18 | 20.79 | 7.83 | 1.32 | 0.19 | 0.15 | 100.35 | 0.79 | 0.35 | −1.45 |
| R204-1.1-1.8 | 37e | 3453.4 | PI | 45.87 | 1.34 | 7.56 | 12.45 | 0.18 | 24.24 | 6.80 | 1.24 | 0.15 | 0.13 | 99.96 | 0.81 | 0.29 | −1.13 |
| R205-7.5-8.15 | 40 | 3458.4 | PI | 45.45 | 1.29 | 7.16 | 12.57 | 0.19 | 25.37 | 6.48 | 1.09 | 0.12 | 0.12 | 99.84 | 0.82 | 0.67 | −1.15 |
| R210-3.3-3.95 | 43 | 3472.2 | HY | 50.38 | 2.15 | 12.60 | 12.13 | 0.19 | 9.67 | 9.86 | 2.20 | 0.30 | 0.26 | 99.73 | 0.64 | 0.66 | −1.69 |
| R219-5.5-7.7 | 44 | 3500.9 | PI | 50.19 | 2.38 | 12.65 | 12.01 | 0.19 | 9.88 | 9.95 | 1.57 | 0.33 | 0.27 | 99.41 | 0.64 | 0.87 | −2.22 |
| R219-8.0-8.8 | 45 | 3505.7 | PI | 49.95 | 2.64 | 14.06 | 12.32 | 0.19 | 6.89 | 11.09 | 2.54 | 0.35 | 0.26 | 100.28 | 0.55 | 0.56 | −1.14 |

[a]Major element analyses are based on ignited (1040°C), volatile-free, samples. $Fe_2O_3$* is total iron expressed as $Fe_2O_3$. Mg# is Mg/(Mg+Fe) after adjusting Fe3+/total Fe to 0.1. LOI is loss on ignition. Alkalic index = total alkali − ($SiO_2$ × 0.37 −14.43). Rock types: PI, pillows; HY, hyaloclastites; MI, massive intrusive units; MV, massive volcanic units.

**Table 1b.** XRF Trace Element Analysis of Lavas Sampled by Phase-2 of the HSDP Core[a]

| Run and Core Interval | Unit | Depth (mbsl) | Rock Type | Nb (ppm) | Zr (ppm) | Y (ppm) | Sr (ppm) | Rb (ppm) | Pb (ppm) | Ga (ppm) | Zn (ppm) | Ni (ppm) | Cr (ppm) | V (ppm) | Ce (ppm) | Ba (ppm) |
|---|---|---|---|---|---|---|---|---|---|---|---|---|---|---|---|---|
| R6-0.85-1.2 | 2a | 3097.7 | PI | 14.9 | 166 | 27.8 | 313 | 7.4 | 1 | 20 | 115 | 134 | 313 | 261 | 30 | 123 |
| R6-2.15-3.0 | 3 | 3098.2 | MI | 11.6 | 117 | 20.8 | 212 | 21.0 | 1 | 17 | 107 | 437 | 534 | 214 | 24 | 103 |
| R8-0.15-0.7 | 2b | 3102.4 | PI | 14.2 | 159 | 27.1 | 311 | 5.8 | 1 | 21 | 113 | 162 | 359 | 262 | 31 | 127 |
| R10-4.35-5.7 | 2d | 3109.4 | PI | 15.1 | 167 | 28.2 | 310 | 6.2 | 1 | 20 | 117 | 139 | 356 | 267 | 32 | 103 |
| R11-5.3-5.7 | 4 | 3111.5 | PB | 14.9 | 165 | 28.0 | 309 | 5.8 | 1 | 21 | 116 | 142 | 369 | 267 | 32 | 99 |
| R13-0.1-0.5 | 5 | 3115.2 | PI | 14.7 | 164 | 27.8 | 311 | 5.9 | 2 | 20 | 113 | 149 | 361 | 265 | 29 | 98 |
| R16-5.2-6.0 | 7 | 3122.5 | PI | 14.5 | 162 | 27.2 | 311 | 5.7 | 1 | 20 | 114 | 166 | 374 | 265 | 32 | 124 |
| R30-4.25-5.2 | 7 | 3141.2 | PI | 14.4 | 160 | 27.1 | 308 | 5.8 | 1 | 20 | 114 | 168 | 364 | 259 | 30 | 120 |
| R51-2.4-3.6 | 9 | 3160.8 | PI | 14.0 | 161 | 27.5 | 316 | 7.7 | 1 | 21 | 112 | 144 | 331 | 261 | 35 | 140 |
| R56-1.0-1.5 | 10 | 3171.1 | PB | 14.7 | 163 | 27.7 | 308 | 5.7 | 1 | 21 | 118 | 155 | 381 | 265 | 27 | 103 |
| R57-5.0-5.9 | 11 | 3173.4 | PI | 14.6 | 163 | 27.6 | 309 | 5.7 | 2 | 20 | 116 | 153 | 359 | 263 | 31 | 111 |
| R60-7.6-8.4 | 13 | 3181.2 | PI | 13.8 | 159 | 27.5 | 314 | 4.8 | 1 | 21 | 113 | 146 | 328 | 259 | 33 | 156 |
| R80-2.8-3.5 | 13 | 3215.5 | PI | 13.8 | 154 | 26.4 | 307 | 5.7 | 2 | 20 | 114 | 140 | 345 | 256 | 27 | 123 |
| R93-1.4-2.0 | 13 | 3234.7 | PI | 13.9 | 154 | 26.6 | 305 | 5.9 | 1 | 20 | 116 | 144 | 366 | 255 | 27 | 123 |
| R101-4.4-4.9 | 14 | 3244.8 | MV | 13.4 | 152 | 26.2 | 309 | 5.9 | 1 | 20 | 111 | 129 | 305 | 248 | 29 | 123 |
| R108-0.0-0.7 | 14 | 3263.9 | MV | 15.0 | 170 | 28.7 | 322 | 7.1 | 1 | 22 | 116 | 120 | 287 | 265 | 32 | 144 |
| R112-7.1-7.7 | 14 | 3277.0 | MV | 13.3 | 150 | 26.6 | 310 | 5.8 | 1 | 21 | 111 | 137 | 310 | 258 | 31 | 123 |
| R116-6.25-7.2 | 15 | 3285.8 | PI | 13.2 | 149 | 26.2 | 311 | 5.7 | 1 | 21 | 111 | 139 | 343 | 255 | 27 | 119 |
| R122-1.85-2.65 | 17 | 3300.1 | PI | 15.9 | 177 | 29.6 | 331 | 8.3 | 1 | 22 | 116 | 87 | 256 | 275 | 36 | 132 |
| R125-4.9-5.3 | 18a | 3305.9 | MI | 14.4 | 161 | 27.1 | 307 | 7.8 | 1 | 20 | 117 | 145 | 383 | 265 | 31 | 104 |
| R127-1.4-2.2 | 19b | 3308.2 | PI | 15.4 | 161 | 26.6 | 335 | 7.8 | 1 | 21 | 113 | 103 | 210 | 266 | 33 | 109 |
| R129-5.8-6.5 | 20b | 3313.5 | MI | 10.2 | 131 | 23.4 | 267 | 3.4 | 1 | 18 | 106 | 378 | 640 | 230 | 25 | 104 |
| R149-1.2-1.6 | 22 | 3333.3 | PI | 15.0 | 163 | 26.0 | 335 | 6.4 | 1 | 21 | 112 | 92 | 199 | 252 | 30 | 102 |
| R154-2.1-2.95 | 23 | 3339.5 | MV | 8.0 | 104 | 18.5 | 221 | 5.0 | 1 | 16 | 105 | 507 | 922 | 194 | 19 | 62 |
| R155-2.7-3.5 | 23 | 3341.4 | MV | 9.3 | 117 | 20.0 | 241 | 2.7 | 2 | 16 | 105 | 698 | 948 | 198 | 22 | 90 |
| R158-1.75-2.10 | 24 | 3348.3 | PB | 15.1 | 163 | 26.2 | 336 | 5.4 | 2 | 21 | 113 | 95 | 206 | 256 | 31 | 97 |
| R162-1.55-2.3 | 25 | 3353.9 | PI | 15.0 | 163 | 25.7 | 329 | 6.3 | 1 | 21 | 114 | 99 | 203 | 255 | 32 | 100 |
| R163-2.1-2.6 | 26 | 3357.0 | HY | 15.0 | 146 | 23.2 | 313 | 4.9 | 2 | 19 | 114 | 185 | 551 | 243 | 31 | 102 |
| R165-0.75-1.45 | 29 | 3359.8 | PI | 14.3 | 144 | 22.8 | 312 | 4.3 | 2 | 18 | 113 | 196 | 593 | 241 | 29 | 87 |
| R168-3.7-4.15 | 30 | 3366.3 | PI | 14.4 | 144 | 22.8 | 318 | 7.4 | 1 | 19 | 111 | 179 | 532 | 236 | 28 | 112 |
| R176-5.93-6.5 | 30 | 3381.3 | PI | 14.3 | 146 | 23.3 | 322 | 5.2 | 2 | 20 | 110 | 173 | 519 | 238 | 28 | 126 |
| R184-1.15-2.1 | 32 | 3400.9 | MI | 12.4 | 131 | 22.2 | 303 | 2.5 | 1 | 19 | 120 | 491 | 647 | 228 | 23 | 95 |
| R187-0.9-2.5 | 33 | 3405.3 | PI | 9.0 | 117 | 20.1 | 234 | 3.0 | 1 | 16 | 105 | 715 | 833 | 194 | 22 | 69 |
| R192-4.4-5.4 | 35 | 3418.1 | MV | 10.1 | 113 | 18.2 | 230 | 2.2 | 2 | 15 | 105 | 979 | 1091 | 178 | 24 | 83 |
| R198-0.5-1.9 | 37a | 3435.2 | PI | 8.7 | 95 | 16.0 | 204 | 3.3 | 1 | 13 | 103 | 935 | 1424 | 168 | 17 | 74 |
| R204-1.1-1.8 | 37e | 3453.4 | PI | 7.5 | 81 | 14.0 | 178 | 2.5 | 1 | 11 | 102 | 1179 | 1653 | 152 | 14 | 52 |
| R205-7.5-8.15 | 40 | 3458.4 | PI | 7.1 | 78 | 13.4 | 165 | 1.9 | 0 | 11 | 103 | 1242 | 1612 | 147 | 16 | 65 |
| R210-3.3-3.95 | 43 | 3472.2 | HY | 10.1 | 153 | 26.3 | 264 | 4.8 | 2 | 19 | 110 | 277 | 548 | 234 | 27 | 66 |
| R219-5.5-7.7 | 44 | 3500.9 | PI | 12.4 | 165 | 26.3 | 313 | 5.6 | 2 | 19 | 108 | 332 | 440 | 240 | 27 | 87 |
| R219-8.0-8.8 | 45 | 3505.7 | PI | 15.1 | 160 | 25.4 | 382 | 3.8 | 2 | 22 | 107 | 98 | 193 | 273 | 37 | 125 |

[a]Rock types: PI, pillows; HY, hyaloclastites; MI, massive intrusive units; MV, massive volcanic units.

**Table 2a.** XRF Major Element Analyses of Phase-1 High CaO Lavas[a]

| Run and Core Interval | Unit | Depth (mbsl) | Rock Type | $SiO_2$ (%) | $TiO_2$ (%) | $Al_2O_3$ (%) | $Fe_2O_3$* (%) | MnO (%) | MgO (%) | CaO (%) | $Na_2O$ (%) | $K_2O$ (%) | $P_2O_5$ (%) | Total (%) | Mg# | LOI (%) | Alkalic Index |
|---|---|---|---|---|---|---|---|---|---|---|---|---|---|---|---|---|---|
| R684-9.0-9.2 | 248 | 1766.7 | HY | 45.50 | 1.89 | 9.29 | 13.08 | 0.20 | 18.80 | 9.44 | 1.41 | 0.54 | 0.19 | 100.34 | 0.76 | 3.34 | −0.43 |
| R685-5.5-6.1 | 248 | 1768.9 | CL | 46.70 | 2.06 | 10.42 | 12.66 | 0.19 | 15.21 | 10.74 | 1.74 | 0.37 | 0.21 | 100.30 | 0.73 | 0.97 | −0.71 |
| R686-3.9-4.1 | 248 | 1771.2 | HY | 46.82 | 2.09 | 10.76 | 12.85 | 0.19 | 15.49 | 9.54 | 1.53 | 0.54 | 0.25 | 100.06 | 0.73 | 9.91 | −0.80 |
| R686-4.5-4.7 | 248 | 1771.3 | CL | 45.90 | 1.87 | 9.52 | 12.82 | 0.19 | 17.95 | 9.90 | 1.46 | 0.27 | 0.20 | 100.08 | 0.75 | 1.25 | −0.80 |
| R686-4.9-5.1 | 248 | 1771.4 | CL | 46.07 | 1.98 | 10.04 | 12.73 | 0.19 | 16.46 | 10.40 | 1.46 | 0.27 | 0.21 | 99.81 | 0.74 | 1.46 | −0.86 |
| R686-7.7-7.9 | 248 | 1772.3 | CL | 46.06 | 1.93 | 9.83 | 12.76 | 0.19 | 16.93 | 10.29 | 1.56 | 0.32 | 0.20 | 100.07 | 0.74 | 0.96 | −0.70 |
| R686-9.5-9.7 | 248 | 1772.8 | CL | 46.08 | 1.96 | 9.76 | 12.80 | 0.19 | 17.04 | 10.26 | 1.49 | 0.31 | 0.20 | 100.09 | 0.75 | 1.18 | −0.79 |
| R687-8.5-8.8 | 248 | 1775.3 | CL | 47.10 | 2.18 | 11.22 | 12.44 | 0.18 | 13.10 | 11.54 | 1.81 | 0.42 | 0.22 | 100.22 | 0.70 | 1.05 | −0.74 |
| R688-0.0-0.4 | 248 | 1775.7 | CL | 45.79 | 1.86 | 9.56 | 12.75 | 0.19 | 17.60 | 9.78 | 1.59 | 0.36 | 0.19 | 99.67 | 0.75 | 1.27 | −0.53 |
| R689-1.2-1.4 | 248 | 1779.1 | CL | 46.01 | 1.82 | 9.39 | 12.95 | 0.19 | 18.26 | 9.17 | 1.56 | 0.47 | 0.18 | 100.00 | 0.76 | 0.79 | −0.54 |
| R689-4.6-4.8 | 248 | 1780.1 | CL | 46.41 | 1.95 | 9.95 | 12.73 | 0.19 | 16.39 | 10.16 | 1.63 | 0.37 | 0.19 | 99.97 | 0.74 | 0.47 | −0.71 |
| R696-1.0-1.6 | 254 | 1794.7 | HY | 45.62 | 1.75 | 8.70 | 13.41 | 0.19 | 21.48 | 7.07 | 1.20 | 0.48 | 0.17 | 100.07 | 0.78 | 5.93 | −0.74 |
| R696-2.1-2.3 | 254 | 1795.4 | CL | 45.73 | 1.67 | 8.66 | 13.01 | 0.19 | 20.66 | 8.41 | 1.21 | 0.42 | 0.17 | 100.13 | 0.78 | 0.09 | −0.83 |
| R696-6.5-6.7 | 254 | 1796.7 | HY | 45.13 | 1.64 | 7.97 | 13.54 | 0.19 | 22.99 | 7.11 | 1.17 | 0.48 | 0.16 | 100.38 | 0.79 | 5.04 | −0.59 |
| R696-9.4-9.6 | 254 | 1797.6 | CL | 46.53 | 1.97 | 10.03 | 12.72 | 0.19 | 16.44 | 10.30 | 1.40 | 0.26 | 0.19 | 100.03 | 0.74 | 1.74 | −1.10 |
| R698-1.4-4.6 | 254 | 1801.2 | CL | 46.65 | 1.87 | 9.75 | 12.74 | 0.19 | 17.43 | 9.83 | 1.45 | 0.25 | 0.19 | 100.35 | 0.75 | 1.65 | −1.10 |
| R698-2.6-2.7 | 254 | 1801.6 | CL | 45.95 | 1.77 | 9.14 | 12.85 | 0.19 | 18.90 | 9.33 | 1.37 | 0.31 | 0.18 | 99.99 | 0.76 | 1.11 | −0.86 |
| R698-8.3-8.5 | 255 | 1803.3 | HY | 46.38 | 1.78 | 9.11 | 13.02 | 0.19 | 19.12 | 8.85 | 0.98 | 0.42 | 0.17 | 100.02 | 0.76 | 2.40 | −1.30 |
| R698-9.1-9.3 | 255 | 1803.6 | HY | 47.52 | 2.09 | 10.96 | 12.56 | 0.18 | 15.46 | 9.35 | 1.27 | 0.39 | 0.20 | 99.98 | 0.73 | 11.26 | −1.47 |
| R699-3.7-4.0 | 255 | 1805.1 | CL | 46.69 | 1.90 | 10.04 | 12.53 | 0.18 | 16.13 | 10.35 | 1.64 | 0.22 | 0.19 | 99.87 | 0.74 | 1.27 | −0.96 |
| R699-5.4-5.6 | 255 | 1805.6 | HY | 46.82 | 1.80 | 9.69 | 12.78 | 0.18 | 17.96 | 9.08 | 1.19 | 0.44 | 0.18 | 100.12 | 0.76 | 3.40 | −1.24 |
| R699-8.4-8.6 | 255 | 1806.5 | HY | 46.56 | 1.72 | 9.29 | 12.83 | 0.19 | 18.81 | 8.91 | 1.40 | 0.31 | 0.16 | 100.18 | 0.76 | 2.34 | −1.06 |
| R700-2.9-3.1 | 255 | 1808.1 | CL | 49.05 | 2.44 | 12.80 | 12.22 | 0.18 | 8.73 | 12.24 | 1.94 | 0.43 | 0.24 | 100.27 | 0.61 | 0.88 | −1.33 |
| R700-3.6-3.8 | 255 | 1808.3 | HY | 47.11 | 1.80 | 9.84 | 12.73 | 0.18 | 17.49 | 9.15 | 1.42 | 0.36 | 0.17 | 100.25 | 0.75 | 2.18 | −1.19 |

[a]Major element analyses are based on ignited (1040°C), volatile-free, samples. $Fe_2O_3$* is total iron expressed as $Fe_2O_3$. Mg# is Mg/(Mg+Fe) after adjusting Fe3+/total Fe to 0.1. LOI is loss on ignition. Alkalic index = total alkali − ($SiO_2$ × 0.37 − 14.43). Rock types: PI, pillows; HY, hyaloclastites; MI, massive intrusive units; MV, massive volcanic units.

**Table 2b.** XRF Trace Element Analyses of Phase-1 High CaO Lavas[a]

| Run and Core Interval | Unit | Depth (mbsl) | Rock Type | Nb (ppm) | Zr (ppm) | Y (ppm) | Sr (ppm) | Rb (ppm) | Pb (ppm) | Ga (ppm) | Zn (ppm) | Ni (ppm) | Cr (ppm) | V (ppm) | Ce (ppm) | Ba (ppm) |
|---|---|---|---|---|---|---|---|---|---|---|---|---|---|---|---|---|
| R684-9.0-9.2 | 248 | 1766.7 | HY | 14.9 | 129 | 15.4 | 295 | 9.6 | 2 | 14 | 98 | 726 | 1470 | 279 | 31 | 186 |
| R685-5.5-6.1 | 248 | 1768.9 | CL | 16.1 | 139 | 17.7 | 360 | 5.1 | 2 | 17 | 100 | 657 | 1407 | 284 | 33 | 147 |
| R686-3.9-4.1 | 248 | 1771.2 | HY | 15.3 | 133 | 17.0 | 322 | 8.1 | 2 | 16 | 94 | 423 | 900 | 289 | 33 | 169 |
| R686-4.5-4.7 | 248 | 1771.3 | CL | 14.7 | 127 | 16.4 | 332 | 1.7 | 2 | 15 | 104 | 833 | 1451 | 276 | 30 | 150 |
| R686-4.9-5.1 | 248 | 1771.4 | CL | 15.6 | 135 | 17.6 | 355 | 2.5 | 3 | 16 | 101 | 709 | 1350 | 281 | 34 | 148 |
| R686-7.7-7.9 | 248 | 1772.3 | CL | 15.4 | 131 | 16.9 | 340 | 4.6 | 2 | 16 | 101 | 748 | 1471 | 285 | 35 | 134 |
| R686-9.5-9.7 | 248 | 1772.8 | CL | 15.1 | 132 | 16.6 | 338 | 3.6 | 1 | 14 | 101 | 767 | 1343 | 277 | 30 | 147 |
| R687-8.5-8.8 | 248 | 1775.3 | CL | 16.9 | 146 | 18.6 | 375 | 5.9 | 2 | 16 | 99 | 551 | 1135 | 281 | 31 | 160 |
| R688-0.0-0.4 | 248 | 1775.7 | CL | 14.3 | 125 | 16.0 | 329 | 4.7 | 2 | 15 | 100 | 816 | 1544 | 250 | 29 | 138 |
| R689-1.2-1.4 | 248 | 1779.1 | CL | 14.7 | 125 | 16.1 | 325 | 7.3 | 2 | 14 | 101 | 785 | 1469 | 265 | 29 | 145 |
| R689-4.6-4.8 | 248 | 1780.1 | CL | 15.5 | 132 | 17.0 | 340 | 4.5 | 1 | 15 | 100 | 715 | 1410 | 269 | 35 | 144 |
| R696-1.0-1.6 | 254 | 1794.7 | HY | 13.2 | 115 | 15.1 | 240 | 7.9 | 2 | 14 | 107 | 792 | 1408 | 254 | 29 | 177 |
| R696-2.1-2.3 | 254 | 1795.4 | CL | 13.5 | 115 | 14.7 | 286 | 6.7 | 1 | 13 | 100 | 965 | 1510 | 225 | 27 | 117 |
| R696-6.5-6.7 | 254 | 1796.7 | HY | 11.9 | 104 | 13.2 | 256 | 9.7 | 5 | 12 | 94 | 790 | 1640 | 277 | 36 | 179 |
| R696-9.4-9.6 | 254 | 1797.6 | CL | 15.2 | 132 | 17.3 | 340 | 2.9 | 2 | 15 | 102 | 688 | 1316 | 272 | 33 | 131 |
| R698-1.4-4.6 | 254 | 1801.2 | CL | 14.2 | 125 | 16.7 | 320 | 2.5 | 2 | 15 | 102 | 798 | 1390 | 259 | 29 | 125 |
| R698-2.6-2.7 | 254 | 1801.6 | CL | 13.7 | 119 | 15.4 | 310 | 3.9 | 2 | 14 | 101 | 864 | 1504 | 259 | 27 | 121 |
| R698-8.3-8.5 | 255 | 1803.3 | HY | 13.5 | 120 | 16.3 | 296 | 6.5 | 2 | 14 | 100 | 714 | 1392 | 252 | 31 | 164 |
| R698-9.1-9.3 | 255 | 1803.6 | HY | 14.5 | 129 | 17.4 | 269 | 5.3 | 2 | 16 | 97 | 370 | 833 | 284 | 31 | 187 |
| R699-3.7-4.0 | 255 | 1805.1 | CL | 14.1 | 128 | 17.9 | 325 | 2.3 | 2 | 15 | 102 | 697 | 1279 | 259 | 29 | 114 |
| R699-5.4-5.6 | 255 | 1805.6 | HY | 12.6 | 117 | 16.6 | 281 | 6.2 | 1 | 14 | 101 | 734 | 1286 | 261 | 28 | 174 |
| R699-8.4-8.6 | 255 | 1806.5 | HY | 11.9 | 114 | 16.6 | 280 | 4.2 | 2 | 14 | 103 | 758 | 1327 | 251 | 25 | 130 |
| R700-2.9-3.1 | 255 | 1808.1 | CL | 18.2 | 165 | 22.4 | 409 | 6.8 | 2 | 19 | 102 | 207 | 598 | 321 | 38 | 158 |
| R700-3.6-3.8 | 255 | 1808.3 | HY | 12.3 | 116 | 17.0 | 279 | 5.2 | 2 | 14 | 104 | 738 | 1369 | 241 | 26 | 128 |

[a]Rock types: HY, hyaloclastites; CL, clasts in hyaloclastites.

**Table 3 (Sample).** ICP-MS Analyses of Lavas Sampled by Phase 2 of HSDP Core [The full Table [3] is available in the HTML version of this article]

| Run and Core | Unit | Sc (ppm) | Rb (ppm) | Sr (ppm) | Y (ppm) | Zr (ppm) | Nb (ppm) | Ba (ppm) | La (ppm) | Ce (ppm) | Pr (ppm) | Nd (ppm) | Sm (ppm) | Eu (ppm) |
|---|---|---|---|---|---|---|---|---|---|---|---|---|---|---|
| R6-0.85-1.2 | 2a | 29 | 7.9 | 308 | 29.7 | 158 | 14.7 | 116 | 12.4 | 31.7 | 4.6 | 21.9 | 5.8 | 1.94 |
| R6-2.15-3.0 | 3 | 27 | 20.1 | 201 | 22.4 | 115 | 11.5 | 84 | 9.1 | 23.2 | 3.4 | 16.2 | 4.3 | 1.46 |
| R8-0.5-0.7 | 2b | 30 | 6.3 | 305 | 28.8 | 154 | 14.0 | 117 | 11.7 | 29.8 | 4.4 | 20.8 | 5.6 | 1.87 |
| R10-4.35-4.7 | 2d | 33 | 6.9 | 313 | 30.6 | 164 | 14.9 | 101 | 12.3 | 31.2 | 4.6 | 21.5 | 5.8 | 1.94 |
| R11-5.3-5.7 | 4 | 33 | 6.9 | 321 | 31.3 | 167 | 15.2 | 99 | 12.3 | 31.3 | 4.6 | 21.5 | 5.8 | 1.96 |
| R13-0.1-0.5 | 5 | 31 | 6.5 | 310 | 30.2 | 160 | 14.6 | 107 | 12.1 | 30.5 | 4.5 | 21.3 | 5.6 | 1.92 |
| R16-5.2-6.0 | 7 | 31 | 6.5 | 313 | 30.0 | 160 | 14.6 | 115 | 12.0 | 30.6 | 4.5 | 21.1 | 5.7 | 1.95 |
| R30-4.25-5.2 | 7 | 32 | 6.5 | 307 | 29.6 | 158 | 14.3 | 107 | 11.9 | 29.9 | 4.4 | 20.9 | 5.6 | 1.92 |
| R51-2.4-3.6 | 9 | 32 | 8.1 | 314 | 30.1 | 161 | 14.7 | 117 | 12.1 | 30.8 | 4.5 | 21.3 | 5.6 | 1.94 |
| R56-1.0-1.5 | 10 | 32 | 6.3 | 307 | 29.5 | 158 | 14.4 | 96 | 11.8 | 30.0 | 4.4 | 21.0 | 5.6 | 1.90 |
| R57-5-5.9 | 11 | 28 | 6.1 | 294 | 28.2 | 152 | 13.8 | 99 | 11.5 | 29.2 | 4.3 | 20.4 | 5.5 | 1.84 |
| R60-7.6-8.4 | 13 | 28 | 5.2 | 299 | 28.1 | 151 | 13.7 | 133 | 11.8 | 29.6 | 4.4 | 20.8 | 5.6 | 1.88 |
| R80-2.8-3.5 | 13 | 31 | 6.3 | 305 | 28.5 | 151 | 13.6 | 110 | 11.4 | 28.8 | 4.3 | 20.1 | 5.4 | 1.84 |
| R93-1.4-2.0 | 13 | 31 | 6.4 | 303 | 28.6 | 151 | 13.7 | 122 | 11.3 | 28.7 | 4.3 | 20.1 | 5.4 | 1.83 |
| R101-4.4-4.9 | 14 | 32 | 6.6 | 307 | 28.8 | 152 | 13.8 | 112 | 11.2 | 28.5 | 4.3 | 20.0 | 5.4 | 1.84 |
| R108-0-0.7 | 14 | 33 | 8.1 | 321 | 31.4 | 169 | 15.3 | 125 | 12.4 | 31.6 | 4.7 | 22.1 | 5.8 | 1.97 |
| R112-7.7-7.7 | 14 | 32 | 6.4 | 299 | 28.2 | 147 | 13.2 | 106 | 11.0 | 28.2 | 4.2 | 19.7 | 5.3 | 1.81 |
| R116-6.25-7.2 | 15 | 33 | 6.5 | 312 | 28.9 | 151 | 13.6 | 102 | 11.2 | 28.4 | 4.2 | 19.7 | 5.4 | 1.83 |
| R122-1.85-2.65 | 17 | 30 | 8.5 | 324 | 31.9 | 173 | 15.8 | 123 | 13.1 | 33.2 | 4.9 | 22.9 | 6.1 | 2.07 |
| R125-4.9-5.3 | 18a | 32 | 8.6 | 309 | 29.9 | 159 | 14.5 | 103 | 11.8 | 30.1 | 4.5 | 21.0 | 5.6 | 1.90 |
| R127-1.4-2.2 | 19b | 32 | 8.4 | 332 | 28.8 | 157 | 15.0 | 105 | 12.1 | 30.9 | 4.5 | 21.2 | 5.6 | 1.87 |
| R129-5.8-6.5 | 20b | 31 | 4.1 | 267 | 25.7 | 131 | 10.4 | 83 | 8.8 | 23.1 | 3.5 | 16.7 | 4.7 | 1.59 |
| R149-1.2-1.6 | 22 | 33 | 7.3 | 336 | 29.7 | 160 | 15.6 | 108 | 12.6 | 31.4 | 4.6 | 21.4 | 5.8 | 1.94 |
| R154-2.1-2.95 | 23 | 25 | 5.2 | 209 | 18.9 | 94 | 7.4 | 57 | 6.6 | 16.7 | 2.6 | 12.3 | 3.5 | 1.21 |
| R155-2.7-3.5 | 23 | 26 | 3.2 | 236 | 22.3 | 112 | 9.6 | 73 | 7.8 | 20.6 | 3.1 | 14.7 | 4.1 | 1.41 |
| R158-1.75-2.10 | 24 | 29 | 6.0 | 315 | 27.1 | 146 | 14.4 | 95 | 11.7 | 29.2 | 4.3 | 19.7 | 5.3 | 1.80 |
| R162-1.55-2.3 | 25 | 32 | 7.1 | 325 | 28.6 | 154 | 15.2 | 106 | 12.1 | 30.3 | 4.4 | 20.7 | 5.5 | 1.89 |
| R163-2.1-2.6 | 26 | 33 | 5.8 | 312 | 25.9 | 141 | 15.2 | 106 | 11.8 | 29.0 | 4.2 | 19.5 | 5.1 | 1.76 |
| R165-0.75-1.45 | 29 | 33 | 5.3 | 321 | 26.1 | 142 | 14.7 | 94 | 11.6 | 29.1 | 4.2 | 19.6 | 5.1 | 1.71 |
| R168-3.7-4.15 | 30 | 33 | 9.2 | 340 | 26.7 | 149 | 15.3 | 126 | 12.3 | 30.3 | 4.4 | 20.3 | 5.2 | 1.80 |
| R176-5.93-6.5 | 30 | 34 | 6.2 | 330 | 26.7 | 148 | 15.3 | 128 | 12.0 | 29.7 | 4.3 | 19.9 | 5.3 | 1.77 |
| R184-1.15-2.1 | 32 | 29 | 3.3 | 310 | 25.1 | 127 | 12.9 | 84 | 9.8 | 24.8 | 3.6 | 17.2 | 4.7 | 1.61 |
| R187-0.9-2.5 | 33 | 27 | 3.6 | 232 | 22.1 | 111 | 9.1 | 69 | 7.5 | 19.8 | 3.0 | 14.4 | 4.0 | 1.40 |
| R192-4.4-5.4 | 35 | 23 | 2.8 | 219 | 19.1 | 106 | 9.9 | 75 | 7.9 | 19.7 | 2.9 | 13.5 | 3.8 | 1.27 |
| R198-0.5-1.9 | 37a | 28 | 3.9 | 208 | 18.0 | 92 | 8.8 | 68 | 7.1 | 18.0 | 2.7 | 12.6 | 3.4 | 1.16 |
| R204-1.1-1.8 | 37e | 24 | 2.9 | 172 | 14.5 | 74 | 7.1 | 48 | 5.5 | 14.3 | 2.1 | 9.9 | 2.8 | 0.94 |
| R205-7.5-8.15 | 40 | 24 | 2.2 | 173 | 15.1 | 79 | 7.6 | 68 | 5.8 | 14.7 | 2.2 | 10.3 | 2.8 | 0.97 |
| R210-3.3-3.95 | 43 | 32 | 5.9 | 275 | 30.5 | 154 | 10.6 | 76 | 10.2 | 26.5 | 4.0 | 19.3 | 5.5 | 1.83 |
| R219-5.5-7.7 | 44 | 30 | 6.4 | 307 | 29.5 | 154 | 12.2 | 90 | 11.3 | 28.5 | 4.3 | 20.2 | 5.5 | 1.85 |
| R222-8.0-8.8 | 45 | 33 | 4.7 | 384 | 29.4 | 158 | 16.2 | 117 | 13.0 | 32.1 | 4.7 | 21.7 | 5.9 | 1.99 |
| BHVO-2, n = 9 | | 31 | 9.6 | 387 | 27.3 | 170 | 18.2 | 130 | 15.1 | 36.6 | 5.3 | 23.9 | 6.1 | 1.98 |
| 1 SD | | 2 | 0.3 | 9 | 0.8 | 4 | 0.4 | 3 | 0.4 | 1.0 | 0.2 | 0.5 | 0.2 | 0.07 |

determined by XRF, we also measured loss on ignition (LOI) on these samples [*Rhodes and Vollinger*, 2004] as an indicator of post-magmatic alteration. LOI is a loss in weight after ignition at 1040°C, reflecting a loss of volatiles which are mostly water and $CO_2$, but also S gases. However, LOI may also record a gain in weight. This is because FeO in minerals and glass are partially oxidized to ferric iron. Therefore with fresh basaltic lavas a LOI measurement can result in a weight gain (or negative LOI).

## 2.2. Solution ICP-MS Analyses of Whole-Rocks

[9] Trace element abundances of the 22 samples from Units 2 to 20 were analyzed using solution ICP-MS at MIT following the method described in the Appendix of *Huang and Frey* [2003], and the 18 samples from Units 22 to 45 were analyzed using solution ICP-MS at Harvard University using the following procedures (Table 3).

**Table 4.** LA-ICP-MS Analyses of High CaO Glasses Sampled by Phase-1 of HSDP Core[a]

| Run and Core | Rb (ppm) | Sr (ppm) | Y (ppm) | Zr (ppm) | Nb (ppm) | Ba (ppm) | La (ppm) | Ce (ppm) | Pr (ppm) | Nd (ppm) | Sm (ppm) | Eu (ppm) | Gd (ppm) | Tb (ppm) | Dy (ppm) | Ho (ppm) | Er (ppm) | Tm (ppm) | Yb (ppm) | Lu (ppm) | Hf (ppm) | Ta (ppm) | Th (ppm) | U (ppm) |
|---|---|---|---|---|---|---|---|---|---|---|---|---|---|---|---|---|---|---|---|---|---|---|---|---|
| R684-8.95 | 16.4 | 474 | 25.8 | 188 | 24.8 | 264 | 21.0 | 56.9 | 7.47 | 30.9 | 7.05 | 2.36 | 6.45 | 0.96 | 5.13 | 0.96 | 2.34 | 0.33 | 1.94 | 0.26 | 4.84 | 1.53 | 1.74 | 0.64 |
| R686-5.10 | 14.1 | 541 | 23.7 | 167 | 22.4 | 235 | 18.4 | 49.8 | 6.51 | 27.0 | 6.22 | 2.12 | 5.74 | 0.86 | 4.68 | 0.87 | 2.16 | 0.30 | 1.77 | 0.24 | 4.27 | 1.36 | 1.60 | 0.59 |
| R689-2.20 | 13.0 | 485 | 22.5 | 156 | 20.4 | 213 | 17.0 | 45.2 | 5.99 | 25.0 | 5.82 | 1.98 | 5.46 | 0.83 | 4.45 | 0.83 | 2.06 | 0.28 | 1.69 | 0.23 | 4.04 | 1.26 | 1.50 | 0.54 |
| R697-8.10 | 11.1 | 481 | 23.2 | 158 | 19.2 | 192 | 16.1 | 39.7 | 5.52 | 23.8 | 5.66 | 1.87 | 5.47 | 0.82 | 4.50 | 0.84 | 2.09 | 0.29 | 1.70 | 0.23 | 4.04 | 1.23 | 1.48 | 0.46 |
| R698-5.60 | 10.6 | 393 | 21.4 | 138 | 17.0 | 170 | 13.6 | 36.0 | 4.99 | 21.5 | 5.23 | 1.76 | 5.13 | 0.77 | 4.19 | 0.78 | 1.95 | 0.27 | 1.62 | 0.22 | 3.59 | 1.08 | 1.22 | 0.43 |
| R699-5.60 | 13.8 | 488 | 24.3 | 165 | 22.4 | 225 | 17.4 | 48.0 | 6.29 | 26.2 | 6.13 | 2.13 | 5.75 | 0.86 | 4.69 | 0.87 | 2.18 | 0.30 | 1.82 | 0.24 | 4.12 | 1.33 | 1.51 | 0.58 |
| R700-1.40 | 10.8 | 451 | 24.5 | 155 | 18.2 | 184 | 15.2 | 39.1 | 5.51 | 24.0 | 5.89 | 2.00 | 5.83 | 0.89 | 4.86 | 0.91 | 2.28 | 0.31 | 1.86 | 0.25 | 4.14 | 1.18 | 1.40 | 0.47 |
| BCR-2g, n = 5 | 49.7 | 353 | 40.6 | 202 | 13.2 | 725 | 25.7 | 55.3 | 7.14 | 28.9 | 6.58 | 1.87 | 6.60 | 1.10 | 6.45 | 1.34 | 3.64 | 0.54 | 3.41 | 0.51 | 4.81 | 0.79 | 6.05 | 1.76 |
| 1 SD | 0.7 | 6 | 1.0 | 5 | 0.2 | 14 | 0.5 | 0.8 | 0.10 | 0.3 | 0.08 | 0.03 | 0.18 | 0.03 | 0.17 | 0.02 | 0.10 | 0.01 | 0.07 | 0.01 | 0.09 | 0.02 | 0.12 | 0.04 |

[a]Major element contents of these glasses were reported by *Stolper et al.* [2004].

[10] About 0.05 g of rock powder was dissolved using 1:1 mixture of HF and $HNO_3$ acids. After complete dissolution, aliquots of solutions were diluted by a factor of 5000 with 1.5% $HNO_3$, and then analyzed for trace element abundances by traditional solution-ICP-MS technique using a GV Quadrupole ICP-MS at Harvard University. The monitored isotopes are in Table A1a of *Huang and Frey* [2003]. USGS standard samples, AGV-1, BCR-1 and BHVO-1, whose trace element abundances are in Table A2 of *Huang and Frey* [2003], were used to construct the standard calibration curve. Each analytical sequence contains three standard sample solutions (BHVO-1, BCR-1 and AGV-1), one procedure blank, four unknown sample solutions, and one BHVO-2 solution analyzed as an unknown sample. In order to monitor the sensitivity drift, beginning with the first solution in the analytical sequence, BHVO-1 solution was analyzed every fifth solution. Each analytical sequence takes about one hour. The sensitivity drifts for all analyzed isotopes are less than 20%, and most are less than 10%. Therefore, no internal drift monitor was used at Harvard. Analytical precision was estimated using multiple measurements (9) of BHVO-2 solution analyzed as an unknown sample during the analyses, and it is better than 5% for all measured trace elements.

## 2.3. LA-ICP-MS Analyses of Glasses

[11] Polished chips of HSDP High Ca-K glasses analyzed for major elements by *Stolper et al.* [2004], were analyzed for trace elements (Table 4) using LA-ICP-MS at Florida State University (FSU). The LA-ICP-MS analysis was conducted using a Finnigan® Element 1 ICP-MS coupled with a New Wave® UP 213 Nd-YAG 213 nm laser system at the National High Magnetic Field Laboratory, FSU. The laser ablation system was used in spot mode with a repetition rate of 10 Hz. The energy output of the laser during the course of analysis was ~1.1 mJ. Trace elements were determined at low resolution (R = 400) using a 100 micron spot size. Each spot was ablated for 75 s. Measured intensity ratios with respect to $^{43}Ca$ were converted to elemental ratios with respect to CaO using BHVO-2g glass standard for calibration. Trace element abundances of BHVO-2 analyzed using solution ICP-MS [*Huang and Frey*, 2003, Table A3] were used for BHVO-2g glass standard. Analytical uncertainty was estimated using multiple measurements (5) of BCR-2g analyzed as an unknown sample during the analyses, and it is better than 3% for all measured trace elements. The reported analytical uncertainties for

**Table 5.** Summary of Olivine Composition in High CaO Lavas[a]

| Unit | Depth (mbsl) | N | Range in Fo% | Mean Fo% | Mean $SiO_2$ | Mean FeO | Mean MnO | Mean MgO | Mean NiO | Mean Total |
|---|---|---|---|---|---|---|---|---|---|---|
| 248 | 1766.7 | 28 | 83.6 to 89.6 | 86.3 ± 1.2 | 40.18 ± 0.28 | 13.30 ± 1.12 | 0.188 ± 0.022 | 46.99 ± 0.82 | 0.375 ± 0.035 | 100.66 ± 0.25 |
| 248 | 1768.9 | 28 | 84.6 to 87.6 | 86.3 ± 0.6 | 40.25 ± 0.14 | 13.30 ± 0.52 | 0.186 ± 0.011 | 46.92 ± 0.41 | 0.368 ± 0.021 | 100.68 ± 0.24 |
| 248 | 1771.4 | 28 | 84.2 to 84.3 | 86.8 ± 0.9 | 40.28 ± 0.18 | 12.60 ± 0.82 | 0.173 ± 0.013 | 46.76 ± 0.67 | 0.387 ± 0.029 | 100.24 ± 0.19 |
| 248 | 1775.3 | 27 | 83.4 to 89.8 | 86.8 ± 1.1 | 40.40 ± 0.23 | 12.70 ± 1.07 | 0.178 ± 0.020 | 47.31 ± 0.83 | 0.396 ± 0.035 | 100.68 ± 0.26 |
| 254 | 1794.7 | 33 | 85.2 to 89.3 | 86.4 ± 1.0 | 40.16 ± 0.20 | 12.90 ± 0.90 | 0.179 ± 0.015 | 46.30 ± 0.65 | 0.361 ± 0.030 | 99.99 ± 0.20 |
| 254 | 1795.4 | 33 | 83.4 to 88.3 | 86.4 ± 1.0 | 40.26 ± 0.14 | 13.00 ± 0.89 | 0.187 ± 0.015 | 46.38 ± 0.67 | 0.365 ± 0.038 | 100.26 ± 0.30 |
| 254 | 1796.7 | 28 | 85.8 to 88.8 | 86.6 ± 0.9 | 40.29 ± 0.18 | 12.96 ± 0.82 | 0.185 ± 0.017 | 46.99 ± 0.61 | 0.389 ± 0.032 | 100.42 ± 0.34 |
| 256 | 1805.6 | 27 | 85.8 to 89.1 | 86.5 ± 0.8 | 40.17 ± 0.25 | 13.03 ± 0.71 | 0.183 ± 0.015 | 47.04 ± 0.57 | 0.375 ± 0.0250 | 100.42 ± 0.17 |
| 256 | 1808.1 | 28 | 81.7 to 87.2 | 86.0 ± 1.3 | 40.12 ± 0.29 | 13.51 ± 1.22 | 0.188 ± 0.016 | 46.49 ± 0.97 | 0.347 ± 0.030 | 100.69 ± 0.21 |
| 256 | 1808.3 | 28 | 86.0 to 89.9 | 87.4 ± 1.1 | 40.37 ± 0.20 | 12.26 ± 1.05 | 0.170 ± 0.020 | 47.69 ± 0.82 | 0.407 ± 0.025 | 100.49 ± 0.21 |

[a]N is number of olivines analyzed. Oxide contents in wt% with 1 standard deviation.

LA-ICP-MS measurements are slightly better than those for solution ICP-MS measurements reported in Section 2.2. The seven HSDP glass chips, as well as the BCR-2g, were analyzed in one LA-ICP-MS analytical session, and their estimated analytical uncertainty reflects the short-term reproducibility within an analytical session, typically less than 6 h. In contrast, the solution ICP-MS measurements for HSDP whole-rock samples include multiple analytical sessions conducted in several days, and the estimated analytical uncertainty for solution ICP-MS measurements reflects the long-term reproducibility.

### 2.4. Electron Microprobe Analyses of Olivine

[12] Major (Si, Mg, Fe) and minor (Mn, Ni) element abundances in olivine phenocrysts were measured simultaneously on the 5-channel Jeol 8200 microprobe at Massachusetts Institute of Technology (Table 5). Each olivine grain was analyzed near the geometric center using a 10 micron wide, 300 nA electron beam, 15 kV accelerating voltage, and 180 s counting time. All element abundances are reported relative to the San Carlos olivine standard using the values reported by *Sobolev et al.* [2007]; CITZAF corrections were applied after *Armstrong* [1995]. Major element abundances were reproducible to better than 0.05%, and minor elements to better than 3–5% (2 s.d.).

## 3. Results

### 3.1. Basalt Classification

[13] A significant result of the Phase-1 HSDP project was the recognition that magmas with distinctly different $SiO_2$ contents, described as "low" and "high" $SiO_2$ were erupted throughout much of the shield-building stage of Mauna Kea volcano [*Stolper et al.*, 2004; *Rhodes and Vollinger*, 2004]. This bimodality has not been observed at other Hawaiian volcanoes. The prevailing opinion has been that individual Hawaiian volcanoes erupt lavas with compositions characteristic of that volcano for a very large part of their eruptive history [e.g., *Garcia et al.*, 1989; *Frey and Rhodes*, 1993]. At Mauna Kea the difference in $SiO_2$ content is most obvious in the glass data, which are clearly bi-modal [*Stolper et al.*, 2004]. The whole-rock data are slightly more ambiguous because of the possible $SiO_2$ loss during alteration, and because of the added complexities of mixing and olivine

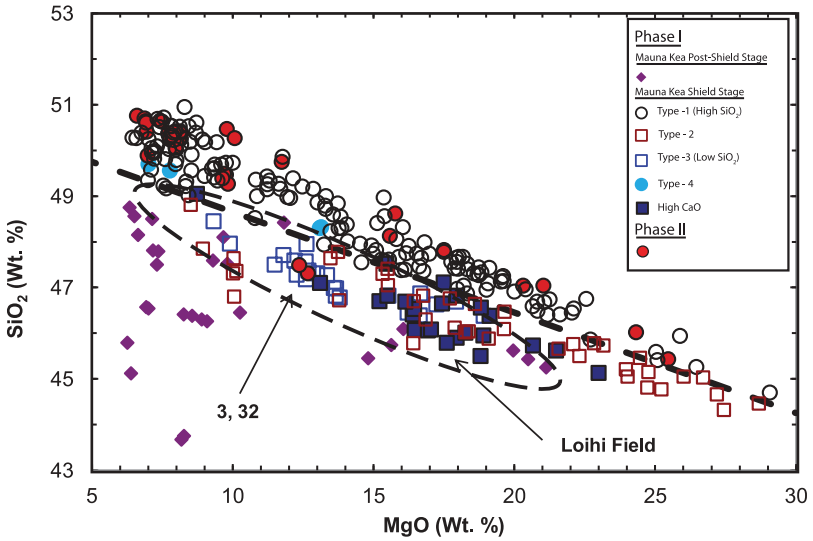


**Figure 2.** Variation of $SiO_2$ and MgO content in HSDP lavas. In Figures 2–14 the data of this study are compared with data for Phase-1 of HSDP [*Rhodes and Vollinger*, 2004; *Huang and Frey*, 2003]. The legend reconciles the classification of *Rhodes and Vollinger* [2004] with that of *Huang and Frey* [2003] (see Table 6). Except for the labeled Phase-2 dikes (units 3 and 32), Phase 2 lavas are high-$SiO_2$. Phase-1 High CaO and post-shield lavas are low-$SiO_2$. The heavy dashed line ($SiO_2 = 50.85 - 0.22 * MgO$) is a discriminant between high and low $SiO_2$ lavas. The dashed field for Loihi tholeiitic lavas is shown for comparison with the low $SiO_2$ Mauna Kea lavas.

accumulation. Nonetheless, as shown in Figure 2, there is a discriminant line between "high" and "low" $SiO_2$ lavas at a given MgO content. This point is emphasized further in a plot of $SiO_2$ normalized to 13% MgO versus depth (Figure 3a).

[14] *Rhodes and Vollinger* [2004] introduced a classificatory scheme for Phase-1 Mauna Kea shield-stage lavas based on normalized $SiO_2$ and Zr/Nb (Figure 4). The normalized $SiO_2$ content (to MgO = 13% and indicated by $SiO_2$ (13)) may reflect depth of melt segregation [*Albarède*, 1992; *Lee et al.*, 2009]. In Hawaiian shield lavas Zr/Nb correlates with radiogenic isotopic ratios [e.g., *Frey and Rhodes*, 1993] and is inferred to reflect geochemical heterogeneity in the source of Mauna Kea shield lavas. Specifically, Type-1 lavas have high $SiO_2$ (13) and high Zr/Nb; Type-2 lavas have low $SiO_2$ (13) and high Zr/Nb; Type-3 lavas have low $SiO_2$ (13) and low Zr/Nb; and rare Type-4 lavas have high $SiO_2$ (13) and low Zr/Nb. This classification differs from that of *Huang and Frey* [2003], mainly with regard to the Type-2 lavas (see Table 6).

[15] With the exception of two intrusive units (3 and 32), all of the flow units from the Phase-2 core are high in $SiO_2$ at a given MgO (Figure 2), and are similar to all other Mauna Kea High $SiO_2$ lavas (Type-1 of *Rhodes and Vollinger* [2004]). Most are pillow lavas with minor hyaloclastites and massive intrusive units (Figure 1a). The two Low $SiO_2$ samples (units 3 and 32) are similar to Low-$SiO_2$ pillow lavas (Type-3 of *Rhodes and Vollinger* [2004]) higher in the section between 2233 and 2481 mbsl. They are intrusive and most probably feeder dikes for the stratigraphically higher Low $SiO_2$ (Type-3) pillow lavas. In this respect, they correspond with other Low $SiO_2$ (Type-3) lavas between 2411 and 3098 mbsl sampled during Phase-1 of the project that are also intrusive [e.g., *Garcia et al.*, 2007].

[16] In an $SiO_2$(13) versus Zr/Nb plot (Figure 4), the two Low $SiO_2$ intrusives (units 3 and 32) have low Zr/Nb, overlapping with Low $SiO_2$ (Type-3) lavas higher in the section. In contrast, the Phase-2 lavas with high $SiO_2$ exhibit a wide range in Zr/Nb which correlates positively with normalized $SiO_2$. The range in Zr/Nb exceeds that for younger High $SiO_2$ lavas higher in the core. The sample from unit 43 has high Zr/Nb (>15) comparable to that of Mauna Loa lavas. The other Phase-2 samples range in Zr/Nb from 9.7–13, with the higher ratios overlapping with the overlying Type-1 (High $SiO_2$) and the lower ratios overlapping with Type-4 lavas (High $SiO_2$ and Zr/Nb < 10 in Figure 4).

[17] Another compositional type of Phase-1 lavas was recognized by *Stolper et al.* [2004], who identified a group of glasses from 1767 to 1808 mbsl that are characterized by high CaO and $K_2O$

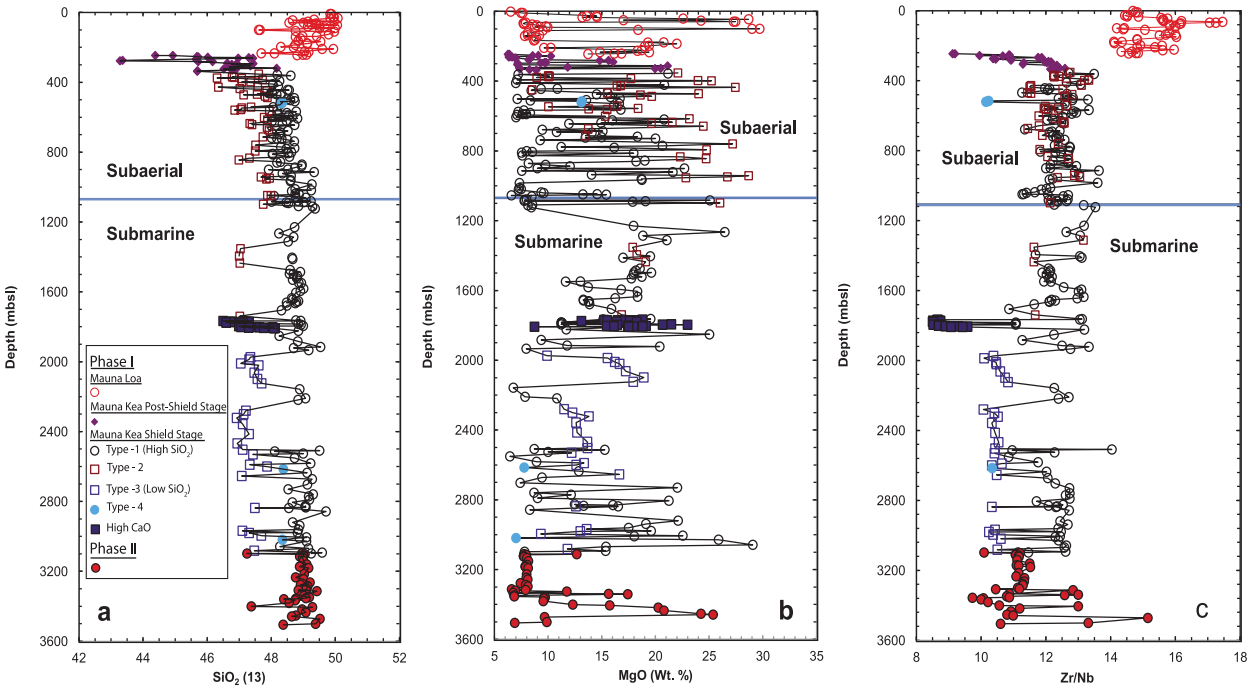


**Figure 3.** Variation with stratigraphic depth (mbsl) of (a) $SiO_2$ normalized to 13% MgO by addition or subtraction of olivine [after *Rhodes and Vollinger*, 2004], (b) MgO, and (c) Zr/Nb.

contents. In this depth interval the hyaloclastites consist of fresh, brown, basaltic glass fragments containing phenocrysts and fragments of olivine. The clast samples have a very fine-grained matrix containing clinopyroxene and plagioclase with phenocrysts of olivine. The olivine phenocrysts and fragments range from $Fo_{83}$ to $Fo_{89}$, but are predominantly $Fo_{86}$ (Table 5). However, no whole-rock samples from this interval were included in the original Phase-1 reference suite samples. Our new

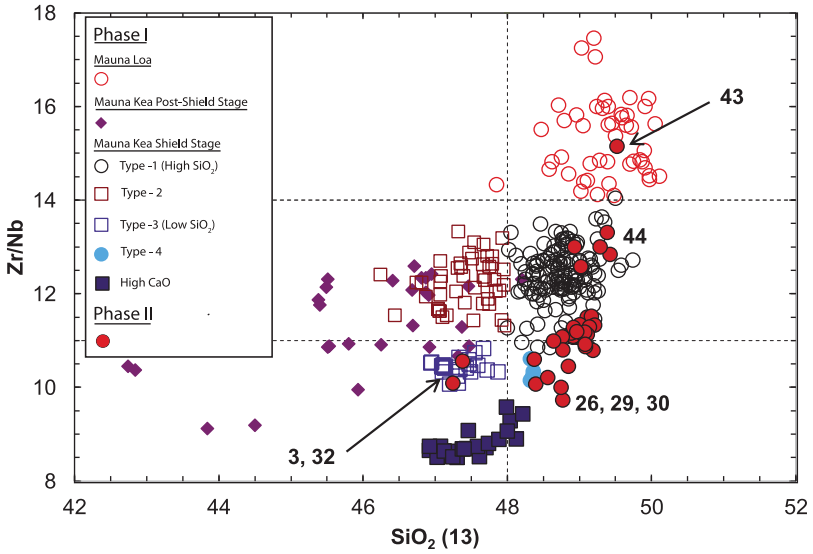


**Figure 4.** Classification of HSDP lavas based on variation of Zr/Nb with $SiO_2$ normalized to 13% MgO by addition or subtraction of olivine. With the exception of units 3 and 32, which correspond with low-$SiO_2$ (Type-3) lavas, the Phase-2 lavas are all high in $SiO_2$, and extend from Type-4 lavas to overlap with Mauna Loa lavas (unit 43). The Phase-1 High CaO lavas have low $SiO_2$ and Zr/Nb and are compositionally distinct. The thin dashed lines distinguish lava types 1, 2, 3 and 4 [*Rhodes and Vollinger*, 2004].

**Table 6.** Comparison of the Different Classifications used by *Rhodes and Vollinger* [2004] and *Huang and Frey* [2003]

| *Rhodes and Vollinger* [2004] | *Huang and Frey* [2003] |
|---|---|
| Type-1 | shield-stage: high $SiO_2$ |
| Type-3 | shield-stage: low $SiO_2$ |
| Type-2 | post-shield tholeiites (low $SiO_2$ above 794 mbsl) |
| Type-4 | not recognized |

analyses of bulk rock samples of clasts and hyaloclastites from this interval have the distinctive high CaO and $K_2O$ contents of glasses in this interval. At a given MgO content, these rocks have higher CaO content and $CaO/Al_2O_3$ than other Mauna Kea tholeiites (Figure 5) and are low in $SiO_2$ at a given MgO (Figure 2). They form a distinct compositional group of lavas with low, but variable, $SiO_2$ (13) and with Zr/Nb of 8.5 to 9.6. Low Zr/Nb values, such as these, are significantly lower than other Mauna Kea tholeiitic basalts, including post-shield tholeiites (Figure 4), but are comparable with post-shield alkalic basalts and highly evolved tholeiites in the uppermost 56 m of the HSDP-1 core [e.g., *Yang et al.*, 1996]. In addition to Zr/Nb, these samples, including glasses previously analyzed for major elements by *Stolper et al.* [2004] are high in incompatible elements such as La, K, Ba, Ce, and Sr. We classify them as a new "High CaO type."

## 3.2. MgO-FeO Relationships

[18] Picritic lavas (MgO > 12%) are common among Hawaiian submarine lavas [e.g., *Garcia et al.*, 1989; *Clague et al.*, 1995; *Garcia et al.*, 1995; *Norman and Garcia*, 1999] and are exceedingly common in the HSDP lavas [*Rhodes and Vollinger*, 2004; *Garcia et al.*, 2007]. Basaltic lavas with around 7–8% MgO, although common, along with picrites, in the subaerial section, are less common in the submarine section. The range in whole-rock MgO for Phase-2 lavas is 6–25%, comparable with the 6–27% found in overlying Phase-1 lavas (Figure 3b). In contrast glass compositions in these lavas range from 6% to 9% [*Stolper et al.*, 2004]. The olivine phenocryst content of Phase-1 lavas varies from as little as 1% to up to 45% [*Garcia et al.*, 2007]. There is a strong correlation of MgO with modal olivine phenocryst abundance [*Garcia et al.*, 2007, Figure 17], a clear indication that the bulk composition of picritic whole-rock compositions are controlled mainly by olivine addition into magmas with lower MgO contents.

[19] However, between 3100 and 3350 mbsl there is a remarkable absence of picrites; in this interval most lavas have between 6–8% MgO (Figure 3b). They are also nearly homogeneous in isotopic ratios of Nd, Hf and Pb [see *Blichert-Toft and Albarède*, 2009, Figure 2]. We suggest that these geochemically similar lavas represent a 250 m interval formed at a relatively high eruption rate from a thoroughly mixed, steady state magma reservoir [e.g., *Rhodes*,

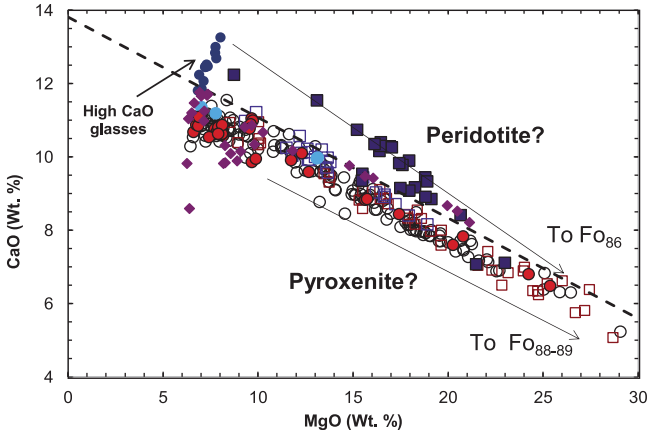


**Figure 5.** Variation of MgO and CaO content in HSDP lavas. The Phase-2 lavas overlap with younger Phase-1 shield tholeiites, but the Phase-1 High CaO lavas (this paper) and glasses [*Stolper et al.*, 2004] are characteristically higher in CaO than other Mauna Kea lavas at a given MgO content. Symbols are as in Figure 4; in addition, High CaO glasses are shown as filled blue circles. The black dashed line is the boundary proposed by *Herzberg* [2006] to distinguish between partial melts of peridotite and pyroxenite. The arrow passing through most of the High CaO data shows the trend for accumulation of olivine $Fo_{86}$ and the arrows parallel to the data for types 1, 2, 3 and 4 show the trend for accumulation of olivine $Fo_{88–89}$.

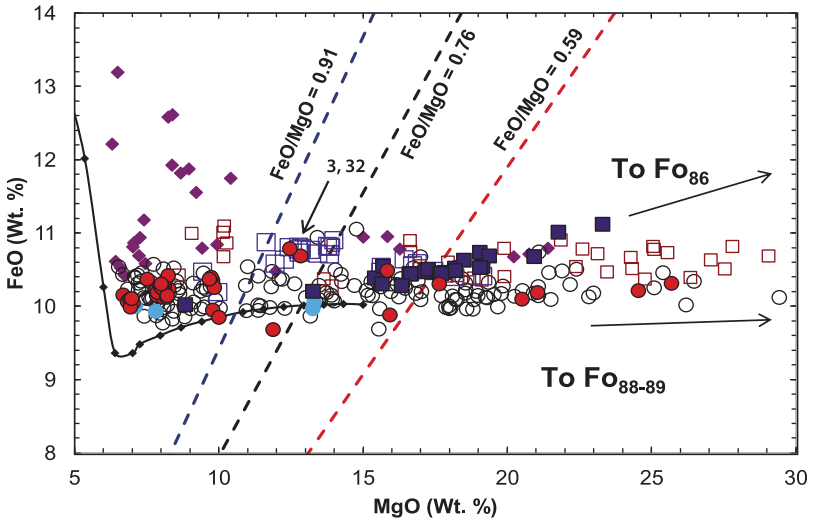


**Figure 6.** FeO versus MgO in HSDP lavas. FeO is calculated from total iron as $Fe_2O_3$ on the assumption that the oxygen fugacity of the lavas was close to magnetite-wüstite (MW) [*Rhodes and Vollinger*, 2005]. The Phase-2 lavas overlap with younger Phase-1 lavas along an almost horizontal trend due to the accumulation of olivine ($Fo_{88–89}$) in melts with lower MgO contents. Although the High CaO lavas also overlap with the Phase-1 lavas they define a steeper trend indicative of accumulation of olivine (~$Fo_{86}$). The three oblique dashed lines represent the FeO/MgO of melts in equilibrium with $Fo_{90.5}$ (red), the maximum Fo content for olivine in these lavas [*Putirka et al.*, 2011]; with $Fo_{89}$ (black), the typical Fo content for olivine in these lavas [*Putirka et al.*, 2011]; and with $Fo_{86}$ (blue), the typical Fo content for olivine in the High CaO lavas (Table 5). The intersection of these lines with the whole-rock trend provides an estimate of the MgO content of parental and possibly primary magmas. Also shown (thin black line with diamonds) is a liquid line of descent for a hypothetical magma with 15% MgO [*Rhodes and Vollinger*, 2004].

1988]. Below 3350 mbsl the MgO variability resembles that in the rest of the core.

[20] Flow units from Phase-2 of HSDP have FeO abundances at a given MgO content comparable with younger Phase-1 lavas (Figure 6). Among the Phase-2 lavas, the two Low $SiO_2$ intrusives (units 3 and 32) have the highest FeO, a result consistent with the relatively high FeO of Low $SiO_2$ (Type-3) lavas higher in the section. The broad sub-horizontal trend in FeO versus MgO (Figure 6) in HSDP shield tholeiites is consistent with the crystallization and accumulation of olivine ($Fo_{87–89}$). Assuming a $K_D$(Fe-Mg) of 0.32 for partitioning between olivine and Mauna Kea melts, lavas crystallizing $Fo_{87–89}$ olivine will have FeO/MgO around 0.76 and contain about 13–15% MgO. *Putirka et al.* [2011] show that both High and Low $SiO_2$ Mauna Kea lavas contain olivine with a maximum forsterite content of $Fo_{90.5}$, indicating possible parental magmas with FeO/MgO around 0.59 containing about 17–18% MgO. Recently, *Matzen et al.* [2011] suggest that a $K_D$(Fe-Mg) of 0.34 for partitioning between olivine and melts is more appropriate for Mauna Kea lavas; in this case the inferred parental magmas will have higher MgO of 18–20%.

[21] The High CaO lavas differ from other compositional types of Mauna Kea lavas in that they define a slightly positive slope in FeO versus MgO (Figure 6). This slope is indicative of crystallization and accumulation of olivine (~$Fo_{86}$), the average olivine composition in these lavas (Table 5). This relatively low Fo olivine is unusual for shield-building Mauna Kea tholeiites [*Baker et al.*, 1996; *Garcia*, 1996; *Putirka et al.*, 2011], requiring a more evolved magma with higher FeO/MgO of around 0.91 and MgO contents of about 11%. In this respect the olivines in the High CaO lavas are similar to olivines in the post-shield lavas with typical forsterite contents of around $Fo_{84–86}$ and maximum values of $Fo_{89}$ [*Baker et al.*, 1996; *Garcia*, 1996; *Putirka et al.*, 2011].

## 3.3. MgO-Ni Relationships

[22] The Phase-2 lavas plot on positive trends of Ni versus MgO that overlap with data from lavas higher in the core (Figure 7). These trends are linear, not curved olivine fractionation trends, providing further evidence that the picritic whole-rock compositions are controlled mainly by olivine addition into magmas with lower MgO contents. The Ni

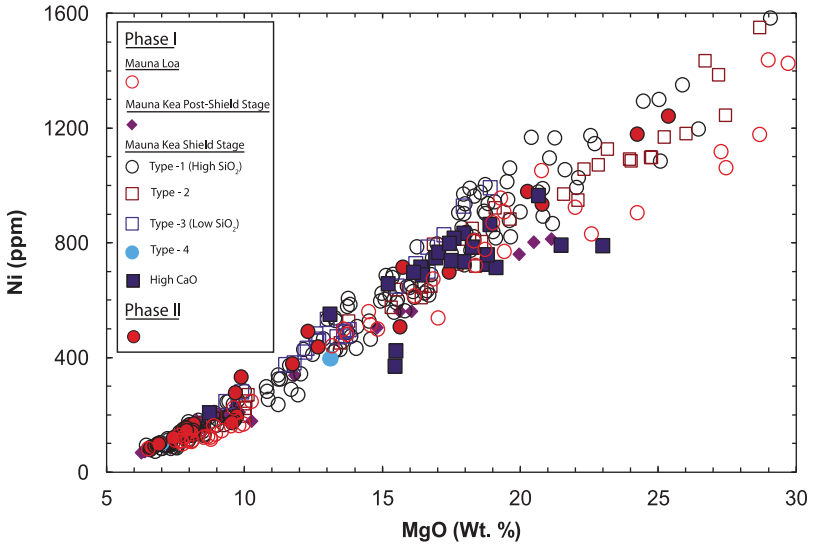


**Figure 7.** Variation in Ni and MgO content in HSDP lavas. The linear trend is indicative of olivine accumulation into melts with lower MgO content. Both Phase-2 lavas and High CaO lavas (with the exception of four hydrated High CaO lavas with >5% LOI; see Table 2a) overlap with Phase-1 lavas. Note that there is no discernable difference in Ni at a given MgO content for lavas with markedly different $SiO_2$ content, including lavas from Mauna Loa.

contents of the Low and High $SiO_2$ lavas are similar at a given MgO content. From this we infer similar Ni contents in olivines from both High and Low $SiO_2$ lavas, an inference that is consistent with the olivine data of *Putirka et al.* [2011]. Ni abundances in the High CaO lavas are also comparable to other shield lavas of similar MgO content, and the Ni content of their olivines (2400–3100 ppm; Table 5) is comparable to other $Fo_{85–86}$ olivines in the core [*Putirka et al.*, 2011]. Four (R686–3.9–4.1, R696–1.0–1.6, R696–6.5–6.7 and R698–9.1–9.3) of the 24 High CaO whole-rocks have lower Ni at a given MgO. Because they have unusually high LOI values (~5 to 11%; Table 2a), we suspect that their anomalously low Ni contents reflect alteration and/or dilution as a result of their high volatile contents.

[23] *Putirka et al.* [2011] propose that both High and Low $SiO_2$ Mauna Kea lavas with around 18% MgO are close to parental magma compositions. Melts with these whole-rock compositions would crystallize olivine corresponding to the most forsteritic olivines ($Fo_{90.5}$) found in these lavas [*Putirka et al.*, 2011, Figure 2]. The Ni content of these proposed parental magmas is around 830 ppm. This estimate is significantly higher than the ~600 ppm Ni proposed by *Sobolev et al.* [2005] and *Herzberg* [2011] for partial melts from fertile peridotite with around 18% MgO.

## 3.4. MgO-CaO Relationships

[24] The CaO content and $CaO/Al_2O_3$ versus MgO content of the Phase-2 lavas are consistent with the crystallization and accumulation of olivine ($Fo_{88–89}$) and are comparable with Phase-1 shield-stage Mauna Kea magmas (Figure 5). Consistent with their steeper FeO versus MgO trend (Figure 6), the whole-rock data for the High CaO samples plot on an olivine ($Fo_{86}$) accumulation trend emanating from the High CaO glass compositions (Figure 5). Like the high CaO - K2O glasses from flow units 248, 254 and 255 [*Stolper et al.* 2004], most of the clasts and hyaloclastites from these units have elevated CaO at a given MgO content (Figure 5) and higher $CaO/Al_2O_3$ (>0.9) than other Mauna Kea shield lavas. The High CaO lavas plot above the line proposed by *Herzberg* [2006] that discriminates magmas derived from peridotites from those produced by melting pyroxenite (Figure 5). According to *Herzberg* [2006, 2011], these rather unusual lavas are the only Mauna Kea shield lavas with a peridotite source; the rest were derived from pyroxenite.

## 3.5. Incompatible Trace Elements

[25] As expected of olivine fractionation and accumulation, abundances of incompatible trace elements are negatively correlated with MgO contents in HSDP lavas (Figures 8a–8c). At a given MgO content, Phase-1 Types 1, 2, 3 and 4 and Phase-2 samples have overlapping incompatible trace element abundances. Relative to other Mauna Kea shield lavas, all of the High CaO samples have higher abundances of incompatible elements (e.g., $K_2O$, Th and Nb), similar abundances of moderately incompatible elements (e.g., $TiO_2$, $P_2O_5$, Zr and Hf)

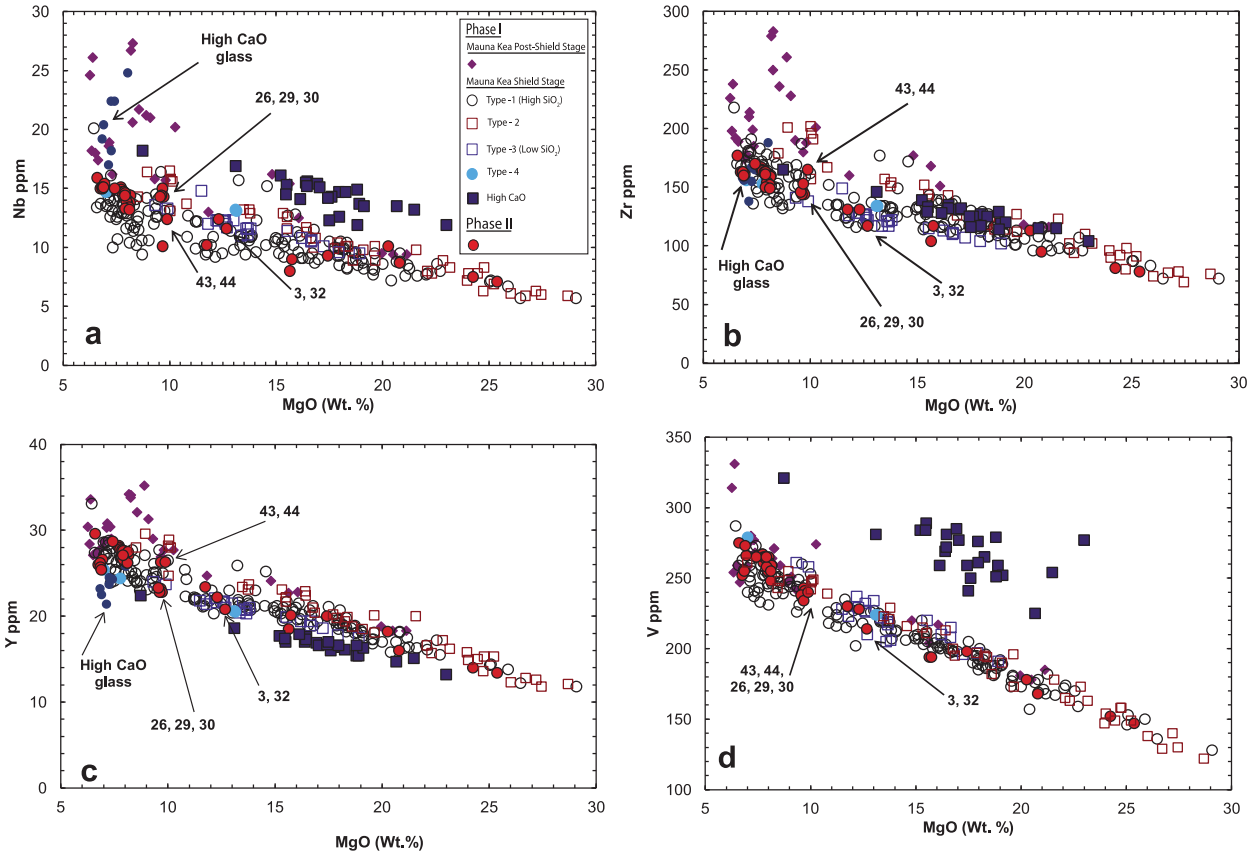


**Figure 8.** Variation of MgO and incompatible element contents in HSDP lavas (a) Nb, (b) Zr, (c) Y, and (d) V. Phase-2 lavas overlap with younger types 2, 2, 3 and 4 Phase-1 lavas; labeled samples are end-members (see Figure 13). In contrast, relative to other Phase-1 lavas the High CaO lavas and their glasses (shown as filled blue circles) are enriched in Nb and V (also K, Ba, Th, La, Ce and Sr) but not in moderately incompatible elements such as Zr and Y (also Ti and P). These results are consistent with a lower extent of melting for the High CaO lavas relative to other Mauna Kea shield tholeiites; see text for details.

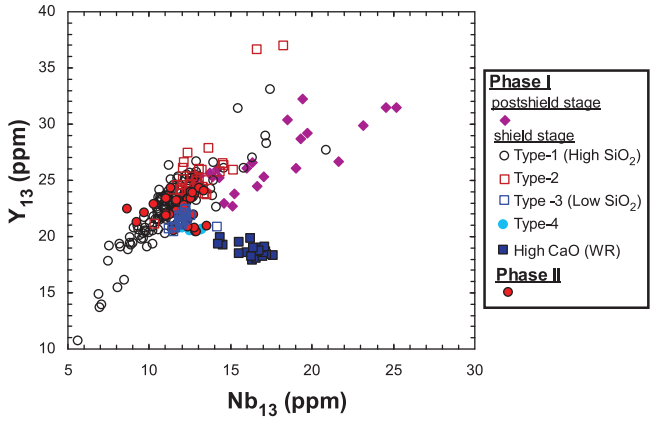


**Figure 9.** Y and Nb contents in HSDP lavas, normalized to MgO = 13%, using a simple MgO-trace element correlation, in order to reduce the effects of crystal fractionation and accumulation of olivine. The High CaO lavas are distinct from all other Phase-1 and -2 lavas in that they define a negative slope that may reflect lower extents of melting in the presence of garnet.

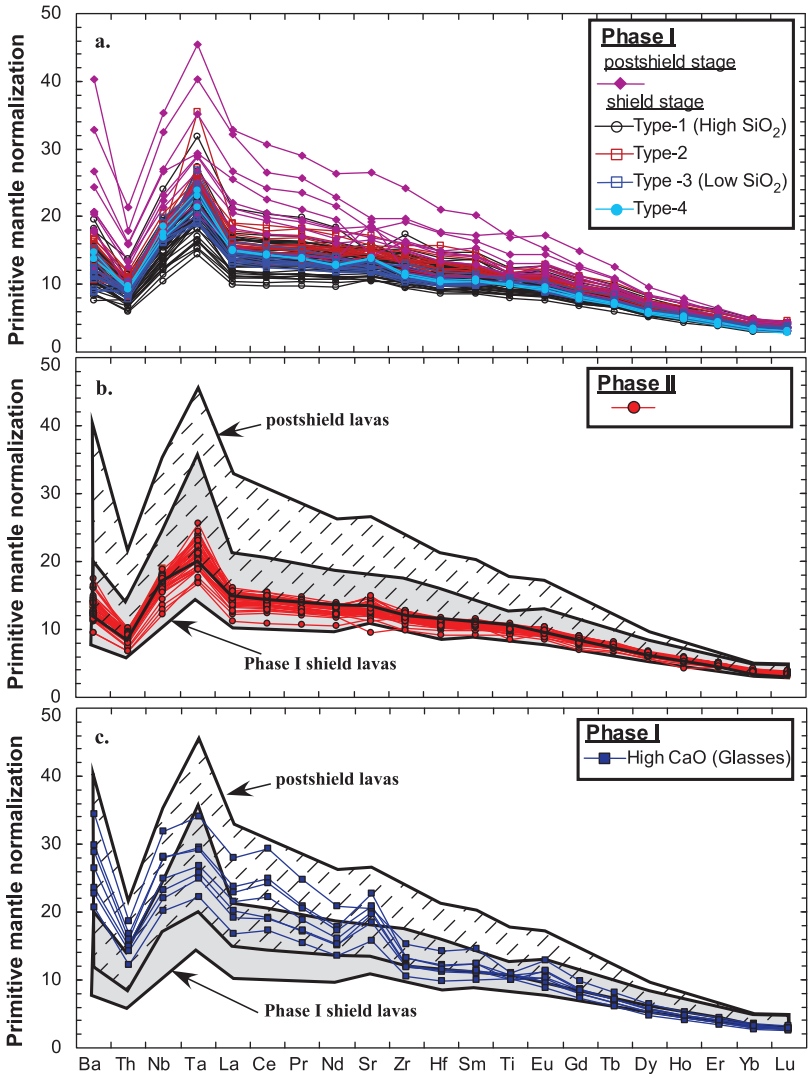


**Figure 10.** Primitive mantle [*McDonough and Sun*, 1995] normalized incompatible element data for HSDP lavas. The data have also been normalized to MgO = 13% to compensate for the effects of crystallization and accumulation of olivine. (a) Phase-1 lavas [*Huang and Frey*, 2003], (b) comparison of Phase-2 lavas (Table 3) with Phase-1 lavas indicated by shaded field, and (c) comparison of Phase-1 High CaO glasses (Table 4) with other Phase-1 lavas. Note the overlap with the diagonal hatched field defined by post-shield lavas.

and lower abundances of Y and HREE (Figures 8 and 10). Important features of the High-CaO lavas are their low Zr/Nb (Figure 4) and an inverse correlation between Nb and Y (Figure 9). They have ratios of Nb/Y, Zr/Y and La/Yb higher than other shield-stage lavas, and have similarities to post-shield lavas (Figure 10c). Their Zr/Nb extend to values lower than the most alkalic post-shield Mauna Kea lavas (Figure 4). The High CaO lavas, however, are not alkalic (alkalinity index ranges from −0.4 to −1.5; Table 1b).

[26] *Stolper et al.* [2004] noted that the High CaO glasses in the 1765–1810 mbsl interval also have high $K_2O$, compared to overlying and underlying shield lavas, but this enrichment of potassium is not accompanied by elevated $TiO_2$ and $P_2O_5$ contents. Our whole-rock analyses of hyaloclastites from this interval are consistent with the glass analyses. Moreover, our results show that $K_2O/P_2O_5$ and $K_2O/TiO_2$ are elevated over a wide range in MgO content, ~7 to 23% (Figure 11). We infer that, in addition to high CaO content, the parental magmas of this group had high $K_2O/P_2O_5$ and $K_2O/TiO_2$. In contrast to the hyaloclastites, the clasts from the 1782–1793 mbsl interval range from high $K_2O/P_2O_5$ and $K_2O/TiO_2$ to lower ratios that overlap with overlying and underlying shield lavas (Figure 11). The considerable scatter in the clasts, 0.11 to 0.26

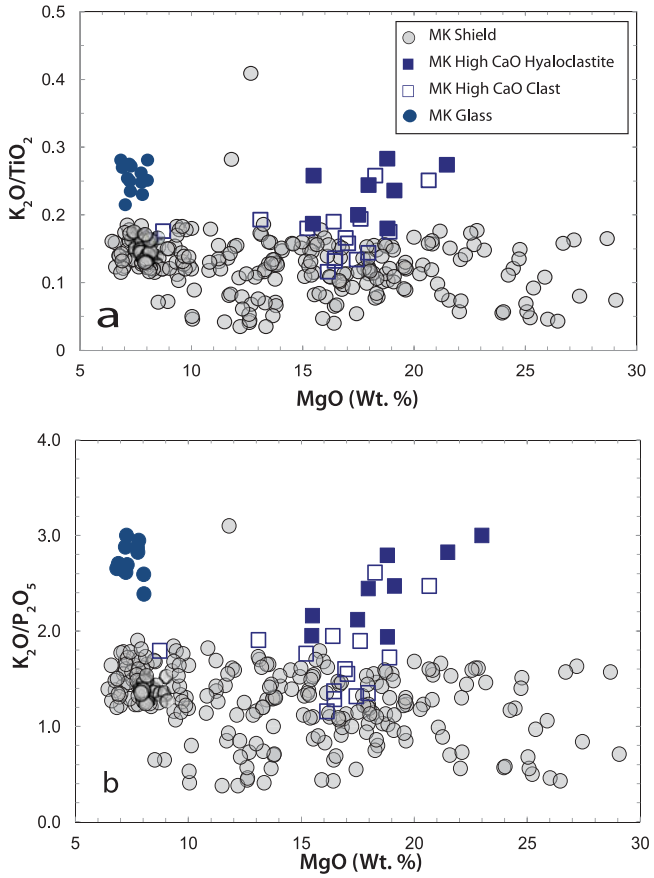


**Figure 11.** Comparison of $K_2O/TiO_2$ and $K_2O/P_2O_5$ in High CaO lavas and glasses (glass data from *Stolper et al.* [2004]) with other compositional types of Mauna Kea shield lavas (indicated by gray circles). The glasses and hyaloclastites have ratios that are higher than the shield lavas, whereas the High CaO clasts range from ratios that overlap with the hyaloclastites and glasses to lower values overlapping with the shield lavas. We interpret the scatter to lower ratios in the shield lavas and some clasts as a consequence of $K_2O$ loss during post-eruption alteration.

in $K_2O/TiO_2$ and 1.1 to 2.5 in $K_2O/P_2O_5$ is comparable with the scatter in other shield lavas and is attributed to post-magmatic alteration caused by interaction with fresh water [see *Huang and Frey*, 2003, Figure 4; *Rhodes and Vollinger*, 2004].

## 4. Discussion

### 4.1. Do Ni Contents in Mauna Kea Lavas Require a Pyroxenite Source?

[27] There was a broad consensus that basaltic magmas result from de-compression melting of a peridotite mantle [e.g., *Yoder and Tilley*, 1962; *Green and Ringwood*, 1967]. Recently, this consensus has been challenged and there is a vigorous debate on the relative roles of peridotite and eclogite/pyroxenite as mantle sources of Hawaiian magmas. For example, *Hauri* [1996] proposed that dacitic magmas, produced from melting lithologically discrete domains of eclogite within the plume, mix with picritic melts of peridotite to produce the range in $SiO_2$ content and isotopic ratios of Hawaiian magmas. Others have adopted variants on this model [e.g., *Takahashi and Nakajima*, 2002; *Huang and Frey*, 2005], particularly in order to explain the high $SiO_2$ content of Makapuu-stage Koolau lavas. Sobolev and colleagues [*Sobolev et al.*, 2005, 2007] have introduced a more complex model in which silicic melts from discrete eclogite domains react with surrounding peridotite to produce secondary pyroxenite. Subsequent melting of differing proportions of these peridotite - pyroxenite hybrids is thought to be responsible for differences in the compositions of Hawaiian magmas, and also for their correlated isotopic and compositional characteristics. *Herzberg* [2006] further argued that most Hawaiian magmas, with the exception of the High CaO Mauna Kea lavas and possibly some Loihi lavas, are derived solely through melting of pyroxenite.

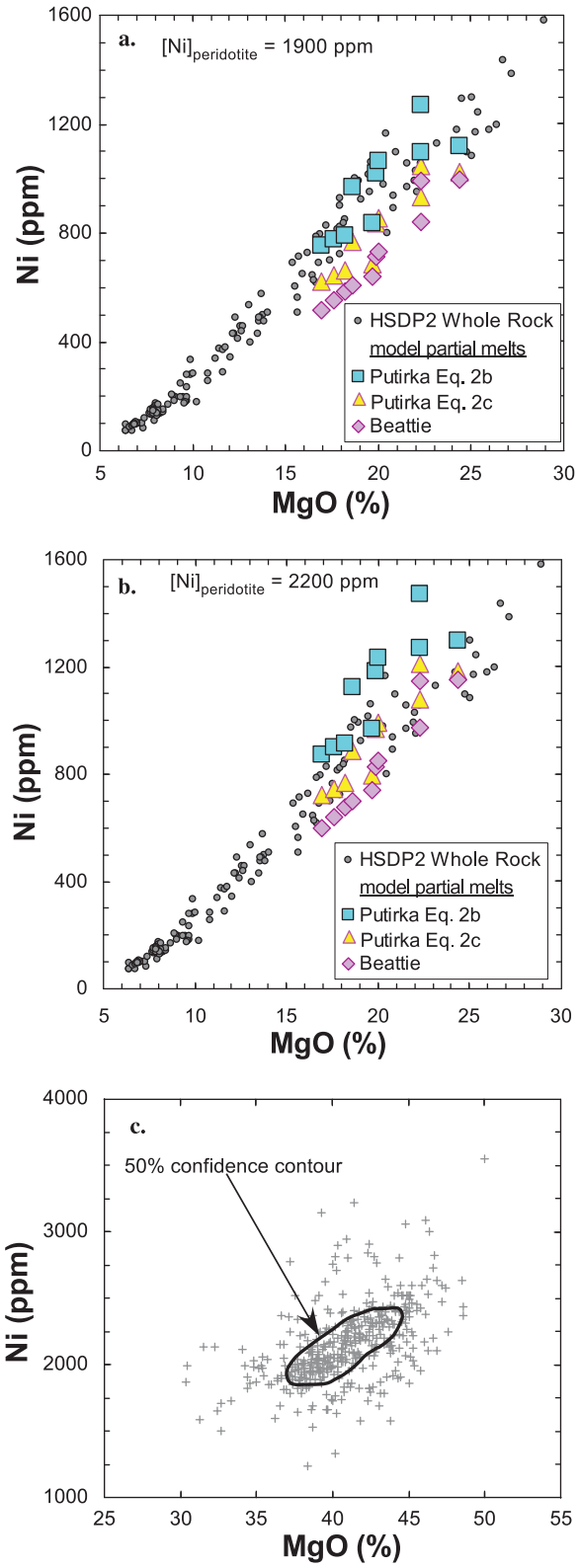


[28] The driving force behind the secondary pyroxenite model is the observation that the Ni contents of olivines in Hawaiian magmas, and therefore their parental melts, are higher than would be expected from melting of peridotite. This discrepancy is most pronounced in lavas with a relatively high $SiO_2$ content. Our whole-rock data, showing similar Ni content at a given MgO in the Low and High $SiO_2$ lavas (Figure 7), are inconsistent with this model, which predicts higher Ni contents in the higher $SiO_2$ lavas (Type-1) relative to the Low $SiO_2$ lavas (Type-2). Similarly, *Putirka et al.* [2011] found comparable Ni contents in the olivines from both High and Low $SiO_2$ lavas. The Ni content of the High CaO lavas (with the exception of four altered samples) overlap the Ni content of other Mauna Kea lavas (Figure 7), as do the Ni content of their olivines (Table 5). If these lavas are derived from peridotite and all other Mauna Kea lavas from pyroxenite, as proposed by *Herzberg* [2006], then according to the *Sobolev et al.* [2005] model they should contain lower Ni at a given MgO. They do not. Additionally, the Ni content, at a given MgO, of Mauna Loa lavas is similar to those of Mauna Kea (Figure 7), despite the higher $SiO_2$ content of the Mauna Loa lavas (Figure 3a). Again this is inconsistent with the *Sobolev et al.* [2005] model.

#### 4.1.1. Ni Partitioning Between Olivine and Melt

[29] Because the Ni content of peridotitic melts is dependent on the Ni content of the peridotite and the $D_{Ni}^{olivine/melt}$, we have re-visited the calculations of *Sobolev et al.* [2005], comparing the results obtained for different models for $D_{Ni}^{olivine/melt}$ and varying the peridotite Ni content (see section A in Text S1 in the auxiliary material and Figures 12a

**Figure 12.** Model calculations for Ni concentrations in partial melts of peridotite. The melting model is identical to that of *Sobolev et al.* [2005] and is based on the (3–5 GPa) melting experiments of *Walter* [1998]. (a) Comparison of Ni versus MgO in Mauna Kea shield-stage tholeiites with calculated partial melts of peridotite containing 1900 ppm Ni. The Ni kd's for olivine/melt are from *Beattie et al.* [1991] and *Putirka et al.* [2011]. (b) Same as in Figure 12a but the Ni content of the source peridotite has been increased to 2200 ppm. (c) Ni versus MgO in 413 peridotites taken from the GeoRoc website (georoc.mpch-mainz.gwdg.de/) and listed in Table S2. There is a wide range in Ni at a given MgO content. A 50% confidence contour shows that the Ni content in peridotites is highly variable and that the assumption of a 2200 ppm source is not unreasonable.

and 12b).[1] Our calculations follow *Sobolev et al.* [2005, Table S1] and are based on the peridotite partial melting (3–5 GPa) experiments of *Walter* [1998]. We used the same $D_{Ni}^{mineral/melt}$ for garnet and pyroxenes as used by *Sobolev et al.* [2005], but for $D_{Ni}^{olivine/melt}$ we used both the *Beattie et al.* [1991] equation, which was used by *Sobolev et al.* [2005], and also equations 2b and 2c from *Putirka et al.* [2011]. The model results are presented in Figure 12a. If the peridotite has 1900 ppm Ni, as proposed by *Sobolev et al.* [2005] and *Herzberg* [2011], then partial melts calculated using the *Beattie et al.* [1991] model should have significantly lower Ni content at a given MgO content than Mauna Kea whole-rocks. This is the original argument of *Sobolev et al.* [2005]. Partial melts calculated using equation 2b of *Putirka et al.* [2011] plot well within the Mauna Kea MgO-Ni whole- rock trend, and melts calculated using equation 2c of *Putirka et al.* [2011] plot slightly below the Mauna Kea whole-rock trend in Figure 12a. Therefore, if equation 2b of *Putirka et al.* [2011] describes the Ni partitioning between olivine and melt during mantle melting more satisfactorily than that of *Beattie et al.* [1991], then the original argument of *Sobolev et al.* [2005] does not hold.

#### 4.1.2. Ni Content in Peridotite

[30] How constant are the Ni contents of mantle peridotites? Is the value of 1900 ppm Ni in fertile peridotite, used by both *Sobolev et al.* [2005] and *Herzberg* [2011], appropriate, or are other values plausible? These questions were addressed by *Putirka et al.* [2011, Appendix A3] and are evaluated in section A in Text S1. The data show a large range in Ni abundances in spinel and garnet peridotites. The mean is 2320 ppm, the median is 2198 ppm, and 50% of the samples are between 2029 and 2400 ppm. Figure 12c, taken from published data on mantle peridotites downloaded from the GeoRoc website (georoc.mpch-mainz.gwdg.de/), shows that at a given MgO content there is considerable Ni variation in peridotite. A 50% confidence contour shows that, in general, MgO and Ni contents are positively correlated, implying that the Ni content in peridotite is mainly controlled by the olivine abundance.

[31] The previous calculations (Figure 12a) followed *Sobolev et al.* [2005] and *Herzberg* [2011] in using "fertile" peridotite with 1900 ppm Ni. However, there is considerable Ni variation at a given MgO content for peridotites (Figure 12c). If we use a Ni content of 2200 ppm for peridotite (which corresponds with the "depleted" peridotite of *Herzberg* [2011] but is well within the 50% confidence contour for peridotite compositions), partial melts calculated using the $D_{Ni}^{olivine/melt}$ model from *Beattie et al.* [1991] overlap with the Mauna Kea whole-rock trend in MgO-Ni (Figure 12b).

[32] Earlier, we showed that the Ni content of Mauna Kea lavas do not follow the predictions of the *Sobolev et al.* [2005] secondary pyroxenite model. There is no relationship between the Ni content of the lavas, or their olivines, and the $SiO_2$ content of HSDP lavas. We conclude, therefore, that because of the large range in the Ni content of possible source peridotites and the current uncertainties in estimating the partitioning of Ni between olivine and melt, there is no compelling reason to accept the model of *Sobolev et al.* [2005] and reject peridotite as the source of Mauna Kea magmas.

### 4.2. Zr/Nb and Pb Isotopic Ratios: Indicators of Geochemical Heterogeneity in the Source of Mauna Kea Shield Lavas

[33] *Eisele et al.* [2003] showed that in a $^{206}Pb/^{204}Pb$ versus $^{208}Pb/^{204}Pb$ plot, HSDP Mauna Kea Phase-1 lavas define three Pb-isotopic arrays that converge at a common, and relatively radiogenic end-point at $^{206}Pb/^{204}Pb \sim 18.7$ and $^{208}Pb/^{204}Pb \sim 38.25$, the Kea end-member of *Tanaka et al.* [2008]. *Eisele et al.* [2003] designated these trends as Hi8, Mid8 and Lo8 to reflect the $^{208}Pb/^{204}Pb$ values at a given value of $^{206}Pb/^{204}Pb$ (Figure 13a). Subsequent studies have confirmed these trends in Phase-2 lavas [*Nobre Silva et al.*, 2008; *Blichert-Toft and Albarède*, 2009]. The simplest explanation is that these trends represent mixing of a single radiogenic end-member with three end-members with relatively low $^{206}Pb/^{204}Pb$, or, more plausibly, a continuum of depleted end-members. Alternatively, the three trends can be explained by a pseudobinary mixing process that involves three components with two components being mixed prior to the addition of the third [e.g., *Bianco et al.*, 2011].

[34] The assignment of an individual sample to the Hi8, Mid8 or Lo8 trends is not always definitive in a $^{206}Pb/^{204}Pb$ versus $^{208}Pb/^{204}Pb$ plot (Figure 13a). *Blichert-Toft and Albarède* [2009] define a parameter $R_C$ based on the slopes of these trends in plots of $^{208}Pb/^{206}Pb$ versus $^{207}Pb/^{206}Pb$, that provides better resolution of the three trends (Figures 13b and 13c). Hi8 lavas have $R_C > 2$, whereas an $R_C$

[1] Auxiliary materials are available in the HTML. doi:10.1029/2011GC003812.

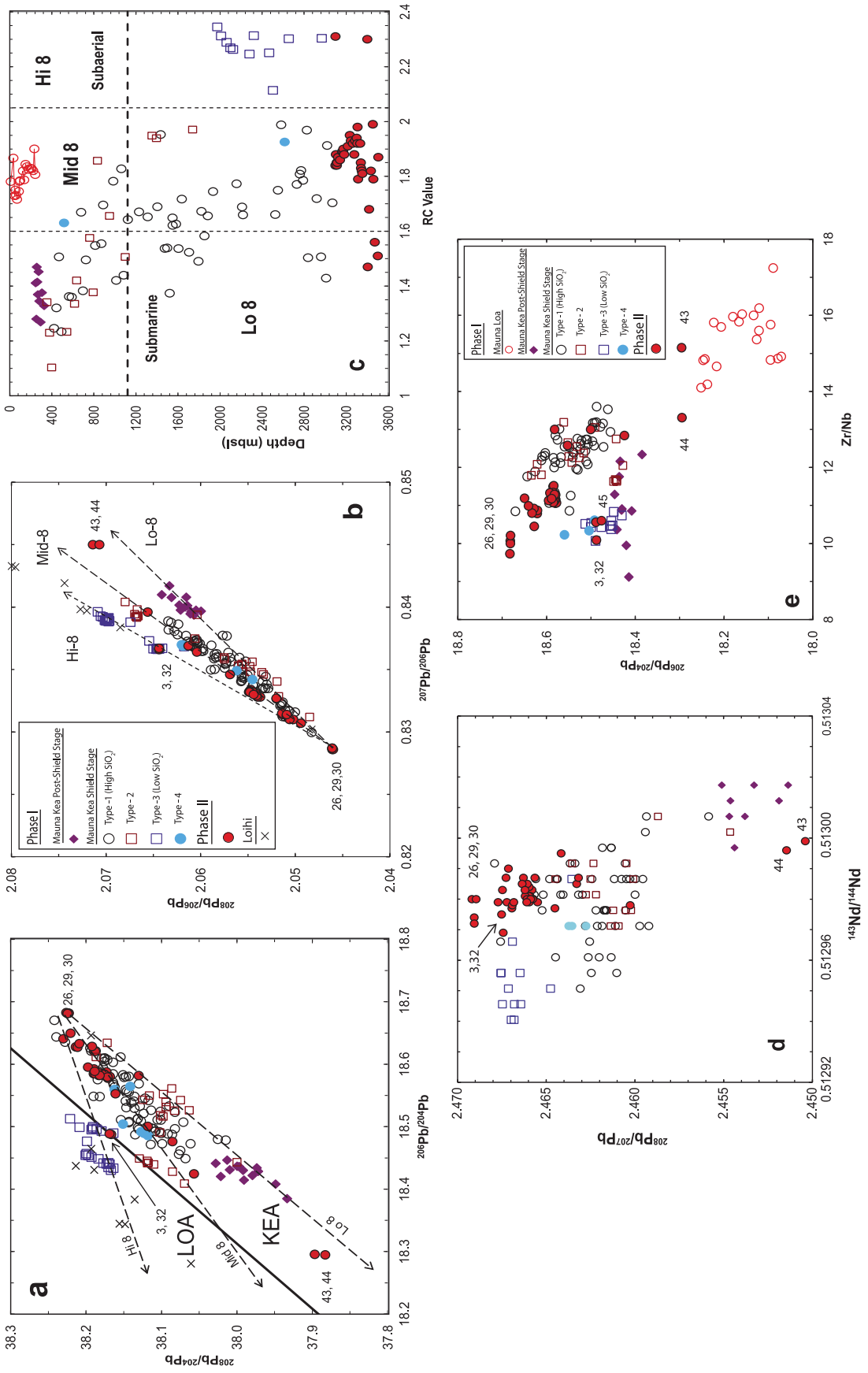
a
b
c
d
e
LOA
KEA
Hi 8
Mid 8
Lo 8
Hi-8
Mid-8
Lo-8
Submarine
Subaerial
Depth (mbsl)
RC Value
Phase I
Mauna Loa
Mauna Kea Post-Shield Stage
Mauna Kea Shield Stage
Type-1 (High SiO2)
Type-2
Type-3 (Low SiO2)
Type-4
Phase II
Loihi
26, 29, 30
3, 32
43, 44
45
Zr/Nb

Figure 13

of ~1.6 separates Lo8 from Mid8 lavas. Lavas with $R_C > 2$ only occur below 1974 mbsl (Figure 13c), and they correspond to the Low-$SiO_2$ group of *Huang and Frey* [2003] and the Type-3 lavas of *Rhodes and Vollinger* [2004].

[35] *Abouchami et al.* [2005], developing an idea originated by *Tatsumoto* [1978], proposed a dividing line that separates lavas erupted at Loa- and Kea-trend Hawaiian volcanoes, with Loa-trend lavas having higher $^{208}Pb/^{204}Pb$ at a given $^{206}Pb/^{204}Pb$ (Figure 13a). All Hi8 lavas plot on the Loa side of the dividing line, defining a mixing trend between the common high $^{206}Pb/^{204}Pb$ Kea end-member with a lower $^{206}Pb/^{204}Pb$ Loa end-member (Figure 13a). Consistent with a mixing interpretation, *Huang and Frey* [2003] found that the Hi8 lavas form a near horizontal Nb/Zr versus La/Yb trend that cannot be explained by partial melting of peridotite (Figure 14). Phase-2 units 3 and 32, the Low $SiO_2$ intrusives (Figures 1a and 2), are within the Hi8 trend at the least radiogenic end of this array (Figure 13a). This high $^{208}Pb/^{204}Pb$ Loa end-member has isotopic and geochemical similarities with Loihi lavas [e.g., *Blichert-Toft et al.*, 2003; *Huang and Frey*, 2003; *Kurz et al.*, 2004; *Rhodes and Vollinger*, 2004].

[36] The High $SiO_2$ lavas that occur throughout the shield-stage of the core belong to both the Mid8 and Lo8 arrays, although the distinction is somewhat arbitrary. The Low $SiO_2$ lavas erupted above 1974 mbsl (Type-2 lavas of *Rhodes and Vollinger* [2004]) also occur on both the Mid8 and Lo8 arrays (Figures 13a and 13b). Most of the Phase-2 lavas plot in the Mid8 field in a tight cluster toward the radiogenic end of the trend, which is defined by Phase-2 units 26, 29 and 30 (Figure 13a). In contrast, Phase-2 units 43 and 44 have the lowest $^{206}Pb/^{204}Pb$ and $^{208}Pb/^{204}Pb$ found in Mauna Kea lavas and plot on the Lo8 array (Figures 13a and 13b). Mauna Kea post-shield lavas fall exclusively on the Lo8 array, and like units 43 and 44 they have relatively non-radiogenic Pb isotopic ratios (Figure 13a). *Frey et al.* [1991] and *Kennedy et al.* [1991] argued that the transition from shield stage volcanism to post-shield stage volcanism at Mauna Kea volcano is characterized by a decreasing degree of partial melting, and an increasing role for a depleted (i.e., high $^{143}Nd/^{144}Nd$, low $^{87}Sr/^{86}Sr$ and low $^{206}Pb/^{204}Pb$, $^{207}Pb/^{204}Pb$ and $^{208}Pb/^{204}Pb$) source component.

[37] The similarity in Pb and Nd isotopic ratios of the relatively young post-shield Mauna Kea lavas and the relatively old units 43 and 44, deep in the shield-stage of the volcano (Figures 13a and 13d) show that the depleted source component sampled during the post-shield stage of volcanism was also sampled early during shield stage volcanism. This indicates that this depleted source component is long-lived and intrinsic to the Hawaiian plume. Similarly, the component with the most radiogenic Pb is present throughout the eruptive history of the volcano, that is, Phase-2 units 26, 29 and 30 and Phase-1 unit 305 (Figures 13a and 13b). It is also evident, from the plot of Rc versus depth (Figure 13c), that the Hi8 (Loihi-like) component with Rc > 2.0) that characterizes the Hi8 Low $SiO_2$ lavas also contributes to both younger high and low $SiO_2$ lavas with Rc = 1.8–2.

[38] Trace element ratios involving Nb, such as Zr/Nb, have long been established as a useful proxy for isotopic ratios in Hawaiian lavas [e.g., *Rhodes et al.*, 1989; *Frey and Rhodes*, 1993; *Frey et al.*, 1994], and in particular for Pb isotopes in Mauna Kea lavas [e.g., *Huang and Frey*, 2003; *Rhodes and Vollinger*, 2004]. There is an overall negative correlation between Zr/Nb and $^{206}Pb/^{204}Pb$ (Figure 13e); that is the depleted component with high Zr/Nb has relatively non-radiogenic Pb isotope ratios. Phase-2 lavas exhibit greater diversity in Pb isotopes [*Nobre Silva et al.*, 2008; *Blichert-Toft and Albarède*, 2009] and Zr/Nb than all of the younger shield-stage lavas recovered during

**Figure 13.** Pb isotopic and Zr/Nb ratios in HSDP lavas. The isotopic data are from *Eisele et al.* [2003], *Blichert-Toft et al.* [2003], *Abouchami et al.* [2005], and *Blichert-Toft and Albarède* [2009]. See legend in Figure 13b for an explanation of the symbols. Several Phase-2 lavas (labeled) have more extreme values than the more numerous Phase-1 lavas. (a) Plot of $^{208}Pb/^{204}Pb$ versus $^{206}Pb/^{204}Pb$ showing the Hi8, Mid8 and Lo8 trends of *Eisele et al.* [2003]. Phase-2 lavas fall on all three trends. Type-3 (low $SiO_2$) lavas define the Hi8 trend and are on the Loa side of the proposed line (shown as a heavy black line) that separates Loa and Kea trend volcanoes [*Abouchami et al.*, 2005]. Loihi data [*Abouchami et al.*, 2005], shown as black crosses, also plot along the Hi8 trend. (b) The same three trends in a plot of $^{208}Pb/^{206}Pb$ versus $^{207}Pb/^{206}Pb$ [*Blichert-Toft and Albarède*, 2009]. (c) Rc versus stratigraphic depth for HSDP lavas. Rc is defined by *Blichert-Toft and Albarède* [2009] and is a parameter based on the slopes of the Hi8, Mid8 and Lo8 trends in a plot of $^{208}Pb/^{206}Pb$ versus $^{207}Pb/^{206}Pb$ (see Figure 13b). Hi8 lavas have Rc > 2.0, Mid8 lavas 1.6 to 2.0, and Lo8 lavas <1.6. (d) Plot showing the inverse correlation of $^{208}Pb/^{207}Pb$ with $^{143}Nd/^{144}Nd$ and the extreme range in the Phase-2 lavas. (e) Plot showing the inverse correlation of $^{206}Pb/^{204}Pb$ with Zr/Nb.

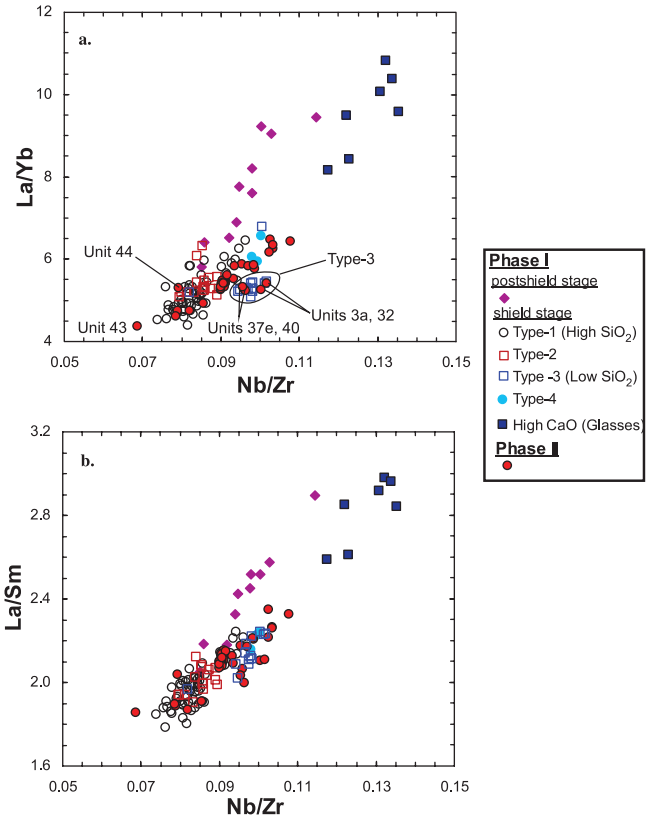


**Figure 14.** Plot of La/Yb and La/Sm versus Nb/Zr for HSDP lavas (data from Tables 3 and 4). The High CaO lavas have higher ratios than other Phase-1 and -2 lavas and are comparable with, and even higher than post-shield lavas. As inferred from Figure 8 their high abundances of highly incompatible elements indicate that the High CaO lavas formed by relatively low degrees of melting.

Phase-1 of HSDP. This is particularly pronounced at the very bottom of the core (>3357 m) where units 26, 29 and 30 have the lowest Zr/Nb (9.7 to 10.1) and the highest $^{206}Pb/^{204}Pb$ (>18.68) and units 43 and 44 have the highest Zr/Nb (13.3 to 15.1) and the lowest $^{206}Pb/^{204}Pb$ (~18.29) (Figure 13e). Units 43 and 44, near the bottom of the core, fall on the Lo8 trend and have the least radiogenic Pb isotopic ratios and highest Zr/Nb, supporting the conclusion that this depleted component was present throughout Mauna Kea's magmatic history, including the post-shield stage. In addition, there are members of all three Pb isotopic trends within the 3098–3506 mbsl part of the core (Figure 13c), thereby implying a wide range of end-member components at this stage in the magmatic history of the volcano.

## 4.3. The Origin of the High CaO Lavas

[39] The High CaO tholeiitic shield basalts occur only over a very narrow stratigraphic range (1767 to 1808 mbsl) and have compositions unlike any other Hawaiian shield tholeiites [*Stolper et al.*, 2004]. *Herzberg* [2006], in a provocative paper, suggested that these High CaO lavas are the only Mauna Kea shield lavas produced by melting of peridotite and that the other types of Mauna Kea shield lavas were derived from melting of pyroxenite.

[40] The High CaO lavas have many similarities to Mauna Kea post-shield lavas. For example, the dominant olivine composition in the High CaO shield lavas is $Fo_{85–86}$, similar to that of post-shield tholeiitic Mauna Kea lavas known as the Hamakua Volcanics (Table 5) [*Baker et al.*, 1996; *Garcia*, 1996; *Putirka et al.*, 2011]. Moreover, oxide versus MgO whole-rock trends for the High CaO shield lavas reflect the accumulation of $Fo_{85–86}$, rather than $Fo_{88–89}$ as is common for other shield-building Mauna Kea tholeiites (e.g., Figures 5 and 6). There are phenocrysts of $Fo_{89}$ in the High CaO shield lavas (Table 5), but these are rare, as they are in post-shield tholeiites. Also, the overlying subaerial post-shield tholeiitic basalts [*Frey et al.*, 1990, 1991] have similarly high CaO and $K_2O$ contents [*Stolper et al.*, 2004, Figure 18d].

[41] In addition, the High CaO shield lavas are characterized by unusually high incompatible element abundances at a given MgO content (Figures 8 and 10) and relatively high ratios of Nb/Zr and La/Yb (Figure 14). These abundances and ratios overlap with those of Mauna Kea's post-shield lavas, and in some samples extend beyond the range of post-shield alkalic lavas (Figures 4 and 14). However, the post-shield lavas do not have the distinctive high $K_2O/TiO_2$ and $K_2O/P_2O_5$ of the High CaO group [*Stolper et al.*, 2004, Figures 18a and 18b].

[42] Currently, there are no isotopic data for the High CaO lavas, but their Zr/Nb, from 8.5 to 9.6, is lower than all other Mauna Kea tholeiites, including post-shield tholeiites. Therefore, based on the inverse trend of Zr/Nb versus $^{206}Pb/^{204}Pb$ (Figure 13e), we predict that their isotopic characteristics will extend the range of Mauna Kea magmas to more radiogenic Pb isotopic ratios, thereby shedding further light on the source characteristics of Mauna Kea lavas.

[43] If we assume similar source compositions for all Mauna Kea shield lavas, several compositional features of the High CaO shield lavas are consistent with their formation by relatively low extents of melting (F), specifically: (1) their relative enrichment in highly incompatible elements, such as Th, K, Nb and La (Figures 8a, 10, 11, and 14); (2) the compatible behavior of Y and relatively low content of heavy rare earth elements in the High CaO lavas (Figures 9 and 10c) which are compatible in garnet and hence their low abundances of these elements suggest that the extent of melting was not sufficient to eliminate garnet from the residue; (3) their high $K_2O/TiO_2$ and $K_2O/P_2O_5$ (Figure 11) is also an expected consequence of low F, <5%, because at low F the low (<1) ratios of mineral/melt compound partition coefficients $D_K/D_{Ti}$ and $D_K/D_P$ for residual garnet and clinopyroxene will create melts with higher $K_2O/TiO_2$ and $K_2O/P_2O_5$ than the source ratios (section B in Text S1); (4) if $D_{CaO}$ for cpx/melt is <1, the CaO content of partial melts of garnet peridotite increase with decreasing F (see case 1 in Figure 6 of *Huang et al.* [2011]), and therefore relatively high CaO content may also reflect relatively low F.

[44] Based on inverse correlations between Sr/Nb and $^{87}Sr/^{86}Sr$ with $\delta^{44/40}Ca$, *Huang et al.* [2011] argued that the Hawaiian plume may contain up to 4% recycled ancient carbonate; the Makapuu-stage of Koolau shield lavas contain the largest amount of this carbonate component. Did the High CaO Mauna Kea lavas have such a carbonate component in their mantle source? We think not because they lack the geochemical characteristics of recycled ancient carbonate component, that is:

[45] (1) The High CaO lavas do not have high Sr/Nb; their Sr/Nb ratios, 19–25, are similar to that of other Mauna Kea tholeiites (16–33);

[46] (2) Two High CaO lavas, R685–5.5–6.1 and R700–2.9–3.1 (labeled as SR685 and SR700 by *Huang et al.* [2011]), have $\delta^{44/40}Ca$ of 0.92 and 0.94. They define the high $\delta^{44/40}Ca_{SRM915a}$ end of the Ca isotopic spectrum of Hawaiian lavas, and are close to the upper mantle values (1.05) defined by measurements on peridotites [*Huang et al.*, 2010].

[47] The high V abundances in High CaO lavas (Figure 8d) are also inconsistent with the source of High CaO lavas being Ca-rich. *Huang et al.* [2011] showed that the net effect of adding carbonate into a peridotite is to increase the clinopyroxene proportion at the expense of orthopyroxene [see *Huang et al.*, 2011, section 5.2 and Table 4]. If the high CaO content in High CaO lavas reflects carbonate in their mantle source (e.g., Case I in Figure 6 and Table 4 of *Huang et al.* [2011]), then a clinopyroxene-rich source is inferred for High CaO lavas. Since V is compatible in clinopyroxene [e.g., *Hart and Dunn*, 1993], the High CaO lavas in equilibrium with abundant clinopyroxene should have relatively low V abundances, which is inconsistent with the higher V abundances in High CaO lavas (Figure 8d).

[48] If the High CaO lavas were derived by lower degrees of melting than the other compositional types of Mauna Kea shield-building tholeiitic basalts, an important implication is that the magma supply to Mauna Kea diminished during the interval, 1765 to 1810 mbsl, of High CaO basalt production. *Stolper et al.* [2004] came to a similar conclusion regarding glasses sampled between 2233 and 2280 mbsl. Although these glasses do not have high CaO, they have relatively high $K_2O$ and $Na_2O$ contents: that is, they are transitional tholeiites formed by relatively low extents of melting. We agree with *Stolper et al.* [2004] that the magma supply to Mauna Kea waxed and waned during the shield-building stage. This is contrary to the common generalization for shield building, where magma supply is represented by a bell-shaped curve of initially increasing, and eventually decreasing magma supply as the volcano migrates toward and away from the plume center [e.g., *Frey et al.*, 1990; *Lipman*, 1995; *DePaolo and Stolper*, 1996].

### 4.4. Does the HSDP-2 Core Include Lavas From Multiple Shields?

[49] The HSDP-2 core sampled an abrupt transition from shield-stage Mauna Loa lavas to older post-shield Mauna Kea lavas at a depth of 245 mbsl [*Rhodes and Vollinger*, 2004]. Were there other inter-shield transitions recorded in the ~695 ka record of the core? Using Pb isotopic data *Eisele et al.* [2003], and more recently *Blichert-Toft and Albarède* [2009] show that there is a tendency for Lo8 lavas to occur high in the core, with Mid 8 lavas below, and inter-layered Hi8 and Mid8 lavas at greater depth (Figure 13c). *Blichert-Toft and Albarède* [2009] suggest that over ~366 ka, Mauna Kea has migrated over three volcanic centers, first Kilauea (Mid8), followed by Loihi-like (Hi8) and finally Mauna Kea (Lo8) as the Pacific Plate moved over the Hawaiian hot spot. This sequence is an oversimplification. Lo8 lavas also occur near the bottom of the core (3472–3501 mbsl) and Mid 8 lavas are found as high as 679 m (Figure 13c). Clearly, all of the geochemical components that contributed to Mauna Kea's magmas were available throughout much of the shield-building history recorded in the core.

[50] The submarine pillows and hyaloclastites of the Hi8 group are Low $SiO_2$ lavas (Type-3), with major, trace and isotopic characteristics similar to those of Loihi magmas [*Rhodes*, 2000; *Huang and Frey*, 2003; *Stolper et al.*, 2004, *Rhodes and Vollinger*, 2004]. They are inter-layered with "normal" High $SiO_2$ (Type-1) Mauna Kea lavas at depths between 1974 and 2481 m. Their estimated ages, based on depth, are around 517–523 ka, a relatively short period of time. Stratigraphically below them, including units 3 and 32 from Phase-2 of HSDP, are intrusive units with similar compositions. They are probably feeders to the overlying extrusive units. These enigmatic lavas present a problem [*Abouchami et al.*, 2005]. They either reflect the presence of relatively short-lived "Loa" source components on the "Kea" side of the plume, or they are lavas from an adjacent volcano with Loa-like isotopic compositions. At that time (~520 ka) it is unlikely that either Loihi or Kilauea were even in existence [*Moore and Clague*, 1992: *DePaolo and Stolper*, 1996; *Lipman et al.*, 2002]. Early, Loihi-like, stages of Mauna Loa or Hualalai are the most compelling candidates. Mauna Loa, however, can be ruled out. Recent Ar/Ar dating of submarine Mauna Loa lavas [*Jicha et al.*, 2009] show that around 500–700 ka Mauna Loa was erupting High-$SiO_2$ lavas, similar to those of modern-day Mauna Loa. Hualalai would have been in a more advanced stage of its evolution than Mauna Loa, making it an even more unlikely candidate.

[51] *Holcomb et al.* [2000] predicted that Kohala lavas would be sampled at depth by the HSDP core because, they argued, the southeast rift zone of Kohala (the Hilo Ridge) extends beneath Mauna Kea. *Lipman and Calvert* [2011] endorse this notion, based on an age of ~1140 ka for transitional tholeiitic lavas dredged from the toe of the Hilo ridge, which, because of their old age, they infer originates from Kohala volcano rather than Mauna Kea. Could these enigmatic Low $SiO_2$ lavas come from Kohala? At this time (~520 ka) Kohala should have been in a vigorous stage of tholeiitic shield-growth [*Moore and Clague*, 1992; *Lipman and Calvert*, 2011] and Phase-2 drilling should have encountered more of these Low $SiO_2$ putative Kohala lavas as it penetrated further into the Kohala shield. It did not. The majority of the Phase-2 lavas are High $SiO_2$ lavas, similar to younger Mauna Kea units, and only two intrusive units (3, 32) are Low $SiO_2$ lavas. Finally, the presence of "Loa" type lavas at Kohala Volcano, which lies along the "Kea" trend, does not solve the problem: it merely shifts the presence of a Loa component to another "Kea" trend volcano.

[52] Recently, *Blichert-Toft and Albarède* [2009] suggested that these Low $SiO_2$ lavas come from a "lost" volcano with strong Loihi affinities. The problem with this alternative interpretation is that the low-$SiO_2$ lavas form a distinct trend (the Hi8 trend of *Eisele et al.* [2003]) in $^{206}Pb/^{204}Pb$ versus $^{208}Pb/^{204}Pb$, converging at the same high radiogenic values of $^{206}Pb/^{204}Pb$ and $^{208}Pb/^{204}Pb$ as the Mid8 and Lo8 Mauna Kea lavas (Figures 13a and 13b). This is unlikely to be a coincidence. Therefore, we conclude that the Low-$SiO_2$ lavas were erupted from Mauna Kea, reflecting the presence of a relatively small-scale, and short-lived, "Loa" heterogeneity within the melting regime of Mauna Kea around 517 to 523 ka. This conclusion is not unprecedented. *Ren et al.* [2005] have shown that melt inclusions in olivine in submarine Haleakala and Koolau lavas have major and trace element characteristics of both "Kea" and "Loa" trend volcanoes. On a larger scale, *Marske et al.* [2007] show that for a brief period between 250–1400 AD the Pb, Sr and Nd isotopic ratios of both Kilauea and Mauna Loa volcanoes shifted from "typical" values, on either side of the Loa-Kea boundary (Figure 13a) toward ratios that were intermediate between the two volcanoes. Subsequently, lavas from both volcanoes returned to more "typical" values. They interpret this transient magmatic event as evidence

for the passage of a small-scale compositional heterogeneity through the melting regimes of both volcanoes. Finally, we predict that, given the distinctive compositional characteristics of the High CaO lavas, such as their low Zr/Nb (Figures 4 and 14), they are likely to have higher $^{206}Pb/^{204}Pb$ and $^{208}Pb/^{204}Pb$ than all the other Mauna Kea shield lavas (Figures 13a and 13d). Are we to infer from this that they too represent lavas from yet another unknown volcano? We think not, and conclude that these isotopic anomalies reflect small-scale source heterogeneities passing through the melting zone of Mauna Kea volcano. Supporting this conclusion we observe that, although Mauna Kea and adjacent Mauna Loa were both in their vigorous shield building stages for much of the last 600 ka [*Jicha et al.*, 2009], there are no Mauna Loa lavas inter-layered with Mauna Kea lavas throughout the entire HSDP core.

## 5. Conclusions

[53] (1) $SiO_2$ and Ni abundance in Hawaiian shield lavas have been used to distinguish between pyroxenite and peridotite sources [e.g., *Sobolev et al.*, 2005]. In the HSDP-2 core there are High and Low $SiO_2$ groups and they have similar Ni contents at a given MgO content. Hence, whole-rock Ni contents in Mauna Kea shield lavas do not reflect differences in source mineralogy for the High and Low $SiO_2$ groups. We conclude that, given the uncertainties in partitioning between olivine and melt, and in the Ni content of peridotites, it is premature to reject peridotite as the mantle source of these magmas.

[54] (2) There is more geochemical diversity, e.g., in Zr/Nb and Pb isotopic ratios, among Mauna Kea Shield lavas in the lower 408 m of the HSDP core than in the overlying 2745 m. of Mauna Kea shield lavas. Clearly, the range of mantle source components that formed the Mauna Kea shield was sampled early, and throughout the growth of the Mauna Kea shield. For example, a depleted component intrinsic to the plume contributed to basalt eruption early in the construction of the shield (units 43 and 44 in the Phase-2 core) and during post-shield volcanism.

[55] (3) A geochemically unique group of High CaO-$K_2O$ lavas first identified by glass composition occur over a narrow depth interval, 1767 to 1808 mbsl in the HSDP core [*Stolper et al.*, 2004]. No whole-rocks from this group have been previously studied, therefore we sampled the core and analyzed hyaloclastites and clasts associated with these compositionally distinct glasses. Relative to other Mauna Kea shield lavas these whole-rocks are also enriched in CaO, $K_2O$ and highly incompatible elements at a given MgO. These shield-stage lavas have affinities with post-shield lavas, for example both groups formed by lower extents of melting than other compositional groups of Mauna Kea shield lavas. Contrary to a previous hypothesis [*Herzberg*, 2006], we find no evidence that these High CaO lavas were derived from a mantle source that was lithologically distinct, that is, peridotite rather than pyroxenite, from the source of other Mauna Kea lavas. The important implication is that melt production waxed and waned during shield growth and large, short-term fluctuations in extent of partial melting are superimposed on the long-term initial increase followed by eventual decrease in melt flux that characterizes growth of a Hawaiian shield as it passes over the Hawaiian plume.

[56] (4) In order to explain the compositional diversity of lavas sampled by the HSDP, it has been suggested that the core contains basalts derived from several volcanoes [e.g., *Blichert-Toft and Albarède*, 2009]. We argue that this is unlikely and we infer that rather than geochemically distinct lavas from several volcanoes, a range of geochemically distinct mantle end-members contributed to basalts forming the Mauna Kea shield.

## Acknowledgments

[57] Special thanks to D. DePaolo, E. Stolper and D. Thomas for initiating, organizing and involving us in the Hawaii Scientific Drilling Project. Also to M. Garcia, E. Haskins and the crew at the rig site for a superb job of core-handling and documentation. E. Stolper and M. Baker generously provided the High CaO glasses whose major element analyses were discussed by *Stolper et al.* [2004]. The paper benefited from thoughtful reviews by D. Weis and J. Bryce. JMR would like to thank Mike Vollinger for the XRF analyses and Pete Dawson for running the XRF lab. SH thanks M. Humayun and V. Salters at FSU and S. Jacobsen at Harvard for access to their ICP-MS facilities and C. Herzberg and K. Putirka for discussions on Ni and Ca partitioning. This research was stimulated by NSF funding for research on HSDP cores (EAR 9528594) but the research discussed in this paper was not NSF funded.

## References

Abouchami, W., A. W. Hofmann, S. J. G. Galer, F. A. Frey, J. Eisele, and M. Feigenson (2005), Pb isotopes reveal bilateral asymmetry in the Hawaiian plume, *Nature*, *434*, 851–856, doi:10.1038/nature03402.

Albarède, F. (1992), How deep do common basaltic magmas form and differentiate?, *J. Geophys. Res.*, *97*, 10,997–11,009, doi:10.1029/91JB02927.

Armstrong, J. T. (1995), CITZAF—A package for correction programs for the quantitative electron microbeam X-ray analysis of thick polished materials, thin-films and particles, *Microbeam Anal.*, *4*, 177–200.

Baker, M. B., S. Alves, and E. M. Stolper (1996), Petrography and petrology of the Hawaii Scientific Drilling Project lavas: Inferences from olivine phenocryst abundances and compositions, *J. Geophys. Res.*, *101*, 11,715–11,727, doi:10.1029/96JB00180.

Beattie, P., C. Ford, and D. Russel (1991), Partition coefficients for olivine-melt and orthopyroxene-melt systems, *Contrib. Mineral. Petrol.*, *109*, 212–224.

Bianco, T. A., G. Ito, J. van Hunen, D. M. Ballmer, and J. J. Mahoney (2011), Geochemical variations at intraplate hot spots caused by variable melting of a veined mantle plume, *Geochem. Geophys. Geosyst.*, *12*, Q0AC13, doi:10.1029/2011GC003658.

Blichert-Toft, J., and F. Albarède (2009), Mixing of isotopic heterogeneities in the Mauna Kea plume Conduit, *Earth Planet. Sci. Lett.*, *282*, 190–200, doi:10.1016/j.epsl.2009.03.015.

Blichert-Toft, J., D. Weis, C. Maerschalk, and F. Albarède (2003), Hawaiian hot spot dynamics as inferred from the Hf and Pb isotope evolution of Mauna Kea volcano, *Geochem. Geophys. Geosyst.*, *4*(2), 8704, doi:10.1029/2002GC000340.

Bryce, J., and D. DePaolo (2005), Geochemical structure of the Hawaiian plume: Sr, Nd, and Os isotopes in the 2.8 km HSDP-2 section of Mauna Kea volcano, *Geochem. Geophys. Geosyst.*, *6*, Q09G18, doi:10.1029/2004GC000809.

Clague, D. A., J. G. Moore, J. E. Dixon, and W. B. Friesen (1995), Petrology of submarine lavas from Kilauea's Puna Ridge, Hawaii, *J. Petrol.*, *36*, 299–349.

DePaolo, D. J., and E. M. Stolper (1996), Models of Hawaiian volcano growth and plume structure: Implications of results from the Hawaii Scientific Drilling Project, *J. Geophys. Res.*, *101*, 11,643–11,654, doi:10.1029/96JB00070.

Eisele, J., W. Abouchami, S. J. G. Galer, and A. W. Hofmann (2003), The 320 kyr Pb isotope evolution of Mauna Kea lavas recorded in the HSDP-2 drill core, *Geochem. Geophys. Geosyst.*, *4*(5), 8710, doi:10.1029/2002GC000339.

Farnetani, C. G., and A. W. Hofmann (2009), Dynamics and internal structure of a lower mantle plume conduit, *Earth Planet. Sci. Lett.*, *282*, 314–322, doi:10.1016/j.epsl.2009.03.035.

Farnetani, C. G., and A. W. Hofmann (2010), Dynamics and internal structure of the Hawaiian plume, *Earth Planet. Sci. Lett.*, *295*, 231–240, doi:10.1016/j.epsl.2010.04.005.

Frey, F. A., and J. M. Rhodes (1993), Inter-shield geochemical differences among Hawaiian volcanoes: Implications for source compositions, melting processes and magma ascent paths, *Philos. Trans. R. Soc. London, Ser. A*, *342*, 121–136, doi:10.1098/rsta.1993.0009.

Frey, F. A., M. O. Garcia, W. S. Wise, A. Kennedy, P. Gurrriet, and F. Alberède (1990), Evolution of Mauna Kea volcano, Hawaii: Petrologic and geochemical constraints on postshield volcanism, *J. Geophys. Res.*, *95*, 1271–1300, doi:10.1029/JB095iB02p01271.

Frey, F. A., W. S. Wise, M. O. Garcia, H. West, S.-T. Kwon, and A. Kennedy (1991), Evolution of Mauna Kea volcano, Hawaii: Petrogenesis of tholeiitic and alkalic basalts, *J. Geophys. Res.*, *96*, 14,347–14,375, doi:10.1029/91JB00940.

Frey, F. A., M. O. Garcia, and M. F. Roden (1994), Geochemical characteristics of Koolau volcano: Implications of intershield geochemical differences among Hawaiian volcanoes, *Geochim. Cosmochim. Acta*, *58*, 1441–1462, doi:10.1016/0016-7037(94)90548-7.

Garcia, M. O. (1996), Petrography and olivine and glass chemistry of lavas from the Hawaii Scientific Drilling Project, *J. Geophys. Res.*, *101*, 11,701–11,713, doi:10.1029/95JB03846.

Garcia, M. O., K. Muenow, J. Aggrey, and J. O'Neil (1989), Major element, volatile, and stable isotope geochemistry of Hawaiian submarine tholeiitic glasses, *J. Geophys. Res.*, *94*, 10,525–10,538, doi:10.1029/JB094iB08p10525.

Garcia, M. O., T. P. Hulsebosch, and J. M. Rhodes (1995), Olivine-rich submarine basalts from the southwest rift zone of Mauna Loa volcano: Implications for magmatic processes and geochemical evolution, in *Mauna Loa Revealed: Structure, Composition, History and Hazards*, *Geophys. Monogr. Ser.*, vol. 92, edited by J. M. Rhodes and J. P. Lockwood, pp. 219–239, AGU, Washington, D. C., doi:10.1029/GM092p0219.

Garcia, M. O., E. H. Haskins, E. M. Stolper, and M. Baker (2007), Stratigraphy of the Hawai'i Scientific Drilling Project core (HSDP2): Anatomy of a Hawaiian shield volcano, *Geochem. Geophys. Geosyst.*, *8*, Q02G20, doi:10.1029/2006GC001379.

Green, D. H., and A. E. Ringwood (1967), The genesis of basaltic magma, *Contrib. Mineral. Petrol.*, *15*, 103–190, doi:10.1007/BF00372052.

Hart, S. R., and T. Dunn (1993), Experimental cpx/melt partitioning of 24 trace elements, *Contrib. Mineral. Petrol.*, *113*, 1–8, doi:10.1007/BF00320827.

Hauri, E. H. (1996), Major-element variability in the Hawaiian mantle plume, *Nature*, *382*, 415–419, doi:10.1038/382415a0.

Herzberg, C. (2006), Petrology and thermal structure of the Hawaiian plume from Mauna Kea volcano, *Nature*, *444*, 605–609, doi:10.1038/nature05254.

Herzberg, C. (2011), Identification of source lithology in the Hawaiian and Canary Islands: Implications for origins, *J. Petrol.*, *52*, 113–146, doi:10.1093/petrology/egq075.

Holcomb, R. T., B. K. Nelson, P. W. Reiners, and N.-L. Sawyer (2000), Overlapping volcanoes: The origin of Hilo Ridge, Hawaii, *Geology*, *28*, 547–550, doi:10.1130/0091-7613(2000)28<547:OVTOOH>2.0.CO;2.

Huang, S., and F. A. Frey (2003), Trace element abundances of Mauna Kea basalt from phase 2 of the Hawaii Scientific Drilling Project: Petrogenetic implications of correlations with major element content and isotopic ratios, *Geochem. Geophys. Geosyst.*, *4*(6), 8711, doi:10.1029/2002GC000322.

Huang, S., and F. A. Frey (2005), Recycled oceanic crust in the Hawaiian Plume: Evidence from temporal geochemical variations within the Koolau shield, *Contrib. Mineral. Petrol.*, *149*, 556–575, doi:10.1007/s00410-005-0664-9.

Huang, S., J. Farkaš, and S. B. Jacobsen (2010), Calcium isotopic fractionation between clinopyroxene and orthopyroxene from mantle peridotites, *Earth Planet. Sci. Lett.*, *292*, 337–344, doi:10.1016/j.epsl.2010.01.042.

Huang, S., J. Farkaš, and S. B. Jacobsen (2011), Stable calcium isotopic compositions of Hawaiian shield lavas: Evidence for recycling of ancient marine carbonates into the mantle, *Geochim. Cosmochim. Acta*, *75*, 4987–4997, doi:10.1016/j.gca.2011.06.010.

Jicha, B., J. M. Rhodes, B. S. Singer, M. J. Vollinger, and M. O. Garcia (2009), $^{40}Ar/^{39}Ar$ geochronology of submarine

Mauna Loa volcano, Hawaii, *Eos Trans. AGU*, *90*(52), Fall Meet. Suppl., Abstract V43F-2328.

Kennedy, A. K., S.-T. Kwon, F. A. Frey, and H. B. West (1991), The isotopic composition of postshield lavas from Mauna Kea volcano, Hawaii, *Earth Planet. Sci. Lett.*, *103*, 339–353, doi:10.1016/0012-821X(91)90171-D.

Kurz, M., J. Curtice, D. Lott, and A. Solow (2004), Rapid helium isotopic variability in Mauna Kea shield lavas from the Hawaiian Scientific Drilling Project, *Geochem. Geophys. Geosyst.*, *5*, Q04G14, doi:10.1029/2002GC000439.

Lee, C.-T., P. Luffi, T. Plank, H. Dalton, and W. P. Leeman (2009), Constraints on the depth and temperatures of basaltic magma generation on Earth and other terrestrial planets using a new barometer for mafic magmas, *Earth Planet. Sci. Lett.*, *279*, 20–33, doi:10.1016/j.epsl.2008.12.020.

Lipman, P. W. (1995), Declining growth of Mauna Loa during the last 100,000 years: Rates of lava accumulation vs gravitational subsidence, in *Mauna Loa Revealed: Structure, Composition, History, and Hazards*, *Geophys. Monogr. Ser.*, vol. 92, edited by J. M. Rhodes and J. P. Lockwood, pp. 45–80, AGU, Washington, D. C., doi:10.1029/GM092p0045.

Lipman, P. W., and A. T. Calvert (2011), Early growth of Kohala volcano and formation of long Hawaiian rift zones, *Geology*, *39*, 659–662, doi:10.1130/G31929.1.

Lipman, P. W., T. W. Sisson, T. Ui, J. Naka, and J. R. Smith (2002), Ancestral submarine growth of Kilauea volcano and instability of its south flank, in *Hawaiian Volcanoes: Deep Underwater Perspectives*, *Geophys. Monogr. Ser.*, vol. 128, edited by E. Takahashi et al., pp. 161–191, AGU, Washington, D. C.

Marske, J. P., A. J. Pietruszka, D. Weis, M. O. Garcia, and J. M. Rhodes (2007), Rapid passage of a small-scale mantle heterogeneity through the melting regions of Kilauea and Mauna Loa volcanoes, *Earth Planet. Sci. Lett.*, *259*, 34–50.

Matzen, A. K., M. B. Baker, J. R. Beckett, and E. M. Stolper (2011), Fe-Mg partitioning between olivine and high-magnesium melts and the nature of Hawaiian parental liquids, *J. Petrol.*, *52*, 1243–1263, doi:10.1093/petrology/egq089.

McDonough, W. F., and S. Sun (1995), The composition of the Earth, *Chem. Geol.*, *120*, 223–253, doi:10.1016/0009-2541(94)00140-4.

Moore, J. G., and D. A. Clague (1992), Volcano growth and the evolution of Hawaii, *Geol. Soc. Am. Bull.*, *104*, 1471–1484, doi:10.1130/0016-7606(1992)104<1471:VGAEOT>2.3.CO;2.

Nobre Silva, I. G., D. Weis, and J. S. Scoates (2008), High-precision isotopic compositions of basalts from the last phase of the Hawaii Scientific Drilling Project, *Geochim. Cosmochim. Acta*, *72*, A687.

Norman, M. D., and M. O. Garcia (1999), Primitive magmas and source characteristics of the Hawaiian plume: Petrology and geochemistry of shield picrites, *Earth Planet. Sci. Lett.*, *168*, 27–44, doi:10.1016/S0012-821X(99)00043-6.

Putirka, K., F. J. Ryerson, M. Perfitt, and W. I. Ridley (2011), Mineralogy and composition of the oceanic mantle, *J. Petrol.*, *52*, 279–313, doi:10.1093/petrology/egq080.

Ren, Z.-Y., S. Ingle, E. Takahashi, N. Hirano, and H. Takafumi (2005), The chemical structure of the Hawaiian mantle plume, *Nature*, *436*, 837–840.

Rhodes, J. M. (1988), Geochemistry of the 1984 Mauna Loa eruption: Implications for magma storage and supply, *J. Geophys. Res.*, *93*, 4453–4466, doi:10.1029/JB093iB05p04453.

Rhodes, J. M. (1996), Geochemical stratigraphy of lava flows sampled by the Hawaii Scientific Drilling Project, *J. Geophys. Res.*, *101*, 11,729–11,746, doi:10.1029/95JB03704.

Rhodes, J. M. (2000), Geochemistry of Mauna Loa and Mauna Kea lavas sampled by the Hawaii Scientific Drilling Project, AGU Fall Meeting, San Francisco, *Eos Trans. AGU*, *81*(48), Fall Meet. Suppl., Abstract V11D-02.

Rhodes, J. M., and M. J. Vollinger (2004), Composition of basaltic lavas sampled by phase-2 of the Hawaii Scientific Drilling Project: Geochemical stratigraphy and magma types, *Geochem. Geophys. Geosyst.*, *5*, Q03G13, doi:10.1029/2002GC000434.

Rhodes, J. M., and M. J. Vollinger (2005), Ferric/ferrous ratios in 1984 Mauna Loa lavas: A contribution to understanding the oxidation state of Hawaiian magmas, *Contrib. Mineral. Petrol.*, *149*, 666–674, doi:10.1007/s00410-005-0662-y.

Rhodes, J. M., K. P. Wenz, C. A. Neal, J. W. Sparks, and J. P. Lockwood (1989), Geochemical evidence for invasion of Kilauea's plumbing system by Mauna Loa magma, *Nature*, *337*, 257–260, doi:10.1038/337257a0.

Sharp, W. D., and P. R. Renne (2005), The $^{40}Ar/^{39}Ar$ and K/Ar dating of lavas, hyaloclastites and intrusions from the HSDP core hole, *Geochem. Geophys. Geosyst.*, *6*, Q04G17, doi:10.1029/2004GC000846.

Sobolev, A. V., A. W. Hofmann, S. V. Sobolev, and I. K. Nikogosian (2005), An olivine free mantle source of Hawaiian shield basalts, *Nature*, *434*, 590–597, doi:10.1038/nature03411.

Sobolev, A. V., et al. (2007), The amount of recycled crust in source of mantle-derived melts, *Nature*, *316*, 412–417.

Stolper, E. M., D. J. DePaolo, and D. M. Thomas (1996), Introduction to special session: Hawaii Scientific Drilling Project, *J. Geophys. Res.*, *101*, 11,593–11,598, doi:10.1029/96JB00332.

Stolper, E. M., S. Sherman, M. Garcia, M. B. Baker, and C. Seaman (2004), Glass in the submarine section of the HSDP2 drill core, Hilo, Hawaii, *Geochem. Geophys. Geosyst.*, *5*, Q07G15, doi:10.1029/2003GC000553.

Stolper, E. M., D. J. DePaolo, and D. M. Thomas (2009), Deep drilling into a mantle plume volcano: The Hawaii Scientific Drilling Project, *Sci. Drill.*, *7*, 4–14.

Takahashi, E., and K. Nakajima (2002), Melting processes in the Hawaiian plume: An experimental study, in *Hawaiian Volcanoes: Deep Underwater Perspectives*, *Geophys. Monogr. Ser.*, vol. 128, edited by E. Takahashi et al., pp. 403–418, AGU, Washington, D. C.

Tanaka, R., A. Makishima, and E. Nakamura (2008), Hawaiian double volcanic chain triggered by an episodic involvement of recycled material: Constraints from temporal Sr-Nd-Hf-Pb isotopic trend of the Loa-type volcanoes, *Earth Planet. Sci. Lett.*, *265*, 450–465, doi:10.1016/j.epsl.2007.10.035.

Tatsumoto, M. (1978), Isotopic composition of lead in oceanic basalt and its implication to mantle evolution, *Earth Planet. Sci. Lett.*, *38*, 63–87, doi:10.1016/0012-821X(78)90126-7.

Walter, M. J. (1998), Melting of garnet peridotite and the origin of komatiite and depleted lithosphere, *J. Petrol.*, *39*, 29–60, doi:10.1093/petrology/39.1.29.

Weis, D., M. O. Garcia, J. M. Rhodes, M. Jellinek, and J. S. Scoates (2011), Role of the Pacific ultra-low velocity zone in generating bilateral asymmetry in the Hawaiian mantle plume, *Nat. Geosci.*, *4*, 831–838, doi:10.1038/ngeo1328.

Yang, H.-J., F. A. Frey, J. M. Rhodes, and M. O. Garcia (1996), Evolution of Mauna Kea volcano: Inferences from lavas recovered in the Hawaii Scientific Drilling Project, *J. Geophys. Res.*, *101*, 11,747–11,767, doi:10.1029/95JB03465.

Yoder, H. S., and C. E. Tilley (1962), Origin of basaltic magmas: An experimental study of natural and synthetic rock systems, *J. Petrol.*, *3*, 342–532.